

<sup>1</sup> **High-resolution regional climate model evaluation using variable-resolution**

<sup>2</sup> **CESM over California**

<sup>3</sup> Xingying Huang, \* Alan M. Rhoades and Paul A. Ullrich

<sup>4</sup> *Department of Land, Air and Water Resources, University of California, Davis*

<sup>5</sup> Colin M. Zarzycki

<sup>6</sup> *National Center for Atmospheric Research*

<sup>7</sup> \*Corresponding author address: Xingying Huang, Department of Land, Air and Water Resources,

<sup>8</sup> University of California Davis, Davis, CA 95616.

<sup>9</sup> E-mail: xyhuang@ucdavis.edu

## ABSTRACT

10 Understanding the effect of climate change at regional scales remains a topic  
11 of intensive research. Computational constraints have meant that the high hor-  
12 izontal resolutions required to reach regional scales have been largely out of  
13 reach of modern global climate models. However, high horizontal resolution  
14 is needed to represent topographic forcing, which is a significant driver of  
15 local climate variability. Although regional climate models (RCMs) have tra-  
16 ditionally been used at these scales, variable-resolution global climate mod-  
17 els (VRGCMs) have recently arisen as an alternative for studying regional  
18 weather and climate. In this paper, the recently developed variable-resolution  
19 option within the Community Earth System Model (CESM) is assessed for  
20 long-term regional climate modeling. The mean climatology of temperature  
21 and precipitation, across California's diverse climate zones, is analyzed and  
22 contrasted with the Weather Research and Forcasting (WRF) model (as a tra-  
23 ditional RCM), regional reanalysis, gridded observational datasets and uni-  
24 form high-resolution CESM with the finite volume (FV) dynamical core. The  
25 results show that variable-resolution CESM is competitive in representing re-  
26 gional climatology on both annual and seasonal time scales. This assessment  
27 adds value to the use of VRGCMs for projecting climate change over the  
28 coming century and improve our understanding of both past and future re-  
29 gional climate related to fine-scale processes. This assessment is also relevant  
30 for addressing the scale limitation of current RCMs or VRGCMs when next-  
31 generation model resolution increases to  $\sim 10\text{km}$  and beyond.

<sup>32</sup> **1. Introduction**

<sup>33</sup> Global climate models (GCMs) have been widely used to simulate both past and future cli-  
<sup>34</sup> mate. Although GCMs have demonstrated the capability to successfully represent large-scale  
<sup>35</sup> features of the climate system, they are usually employed at coarse resolutions ( $\sim 1^\circ$ ), largely  
<sup>36</sup> due to computational limitations. Global climate reanalysis datasets, which assimilate climate  
<sup>37</sup> observations using a global model, represent a best estimate of historical weather patterns, but  
<sup>38</sup> still have relatively low resolutions no finer than  $0.5^\circ$  (<http://reanalyses.org/atmosphere/>  
<sup>39</sup>) overview-current-reanalyses). Consequently, regional climate is not well captured by ei-  
<sup>40</sup> ther GCMs or global reanalysis datasets. However, dynamical processes at unrepresented scales  
<sup>41</sup> are significant drivers for regional and local climate variability, especially over complex terrain  
<sup>42</sup> (Soares et al. 2012). In order to capture these fine-scale dynamical features, high horizontal reso-  
<sup>43</sup> lution is needed to allow for a more accurate representation of fine-scale forcings, processes and  
<sup>44</sup> interactions (Leung et al. 2003a; Rauscher et al. 2010). We anticipate that with these enhancements  
<sup>45</sup> the regional climate information will be more usable for policy makers and local stakeholders in  
<sup>46</sup> formulating climate adaptation and mitigation strategies.

<sup>47</sup> In order to model regional climate at high spatial and temporal resolution over a limited area,  
<sup>48</sup> downscaling methods have been developed. There are largely two approaches for downscaling:  
<sup>49</sup> The first is statistical downscaling, which aims to estimate fine scale behavior via analysis of the  
<sup>50</sup> statistical relationships between observed small-scale variables and larger (GCM) scale variables  
<sup>51</sup> (Fowler et al. 2007). This method is empirical and cannot be used if the observed relationships  
<sup>52</sup> do not hold with a changing climate (Soares et al. 2012). The second approach is dynamical  
<sup>53</sup> downscaling, which uses a numerical model to simulate higher spatial resolution conditions in  
<sup>54</sup> greater detail. Dynamical downscaling is popular and commonly employed using nested limited-

area models (LAMs) or by using a variable resolution GCM (VRGCM) to model regional scales (Laprise 2008). In this context, LAMs are typically referred as regional climate models (RCMs) when applied to climate scales. RCMs are forced by output of GCMs or reanalysis data, and have been widely used, particularly to capture physically consistent regional and local circulations at the needed spatial and temporal scales (Christensen et al. 2007; Bukovsky and Karoly 2009; Mearns et al. 2012). Recently, VRGCMs have been increasingly employed for modeling regional climate. This approach uses a global model that includes high-resolution over a specific region and lower resolution over the remainder of the globe (Staniforth and Mitchell 1978; Fox-Rabinovitz et al. 1997). Within VRGCM, there are also different strategies of achieving high-resolution over the area of interest such as stretched-grid models or grid refinement (Fox-Rabinovitz et al. 1997; Zarzycki et al. 2015). VRGCMs have been demonstrated to be effective for regional climate studies and applications, owing to the advantages of traditional GCMs in representing large-scale features, at a reduced computational cost compared to uniform GCMs (Fox-Rabinovitz et al. 2001, 2006; Rauscher et al. 2013; Zarzycki et al. 2014; Zarzycki and Jablonowski 2014; Zarzycki et al. 2015). Fox et al. (2000) found that the stretched-grid version of a GCM simulated not only large-scale but also mesoscale features especially when considering orographic forcing (Fox-Rabinovitz et al. 2000).

Compared with RCMs, a key advantage of VRGCMs is that they use a single, unified modeling framework, rather than a separate GCM and RCM. Thus, VRGCMs avoid potential inconsistency between the global and regional domains, and naturally support two-way interaction between these domains without the need for nudging (Warner et al. 1997; McDonald 2003; Laprise et al. 2008; Mesinger and Veljovic 2013). However, in order to obtain deeper insight into the performance of these two modeling approaches, it is necessary to compare them directly. For the purposes of this paper, we will focus on the recently developed variable-resolution Community Earth System

79 Model (varres-CESM) using the grid refinement technique as our VRGCM of interest. Although  
80 CESM has been well-used for uniform resolution modeling, variable-resolution in the Commu-  
81 nity Atmosphere Models (CAM) Spectral Element (SE) dynamical core has only been recently  
82 developed. Zarzycki et al. (2014) applied this option in CAM-SE and showed that high-resolution  
83 simulation of topical cyclones represented significant improvements over the unrefined simulation  
84 (Zarzycki et al. 2014). Zarzycki et al. also compared the large-scale features of varres-CESM  
85 0.25° and uniform CESM at 1 degree, and found that adding refined region over the globe did not  
86 affect the global circulation noticeably (Zarzycki and Jablonowski 2014; Zarzycki et al. 2015).

87 However, varres-CESM has yet to be rigorously investigated for long-term regional climate sim-  
88 ulation (Taylor and Fournier 2010; Zarzycki et al. 2014). And in this paper, it is the first time to  
89 investigate whether VRGCMs can show similar or even better ability in regional climate modeling  
90 compared with traditional method of RCMs. Consequently, the goal of this paper is to evaluate  
91 the performance of varres-CESM against gridded observational data, reanalysis data and in com-  
92 parison to a RCM. Also, outputs from a uniform high-resolution CESM simulation have been  
93 utilized here Wehner et al. (2014a). Our variable-resolution simulations will focus on relatively  
94 high resolutions for climate assessment, namely 28km and 14km regional resolution, which are  
95 much more typical for dynamically downscaled studies. For comparison with the more widely  
96 used RCM method, the Weather Research and Forecasting (WRF) model will be used (Skamarock  
97 et al. 2005). The study focuses on models' ability to represent current climate statistics, partic-  
98 ularly those relative to climate extremes. We anticipate that this assessment will add value in  
99 modeling mean regional climatology and improve our understanding about the effects of multi-  
100 scale processes in regional climate regulation. Our goal is also to advance the understanding of  
101 better use of models in future climate predictions and climatic extremes studies regionally.

With its complex topography, coastal influences, and wide latitudinal range, this makes CA an excellent test bed for high-resolution climate studies. Also, an understanding of local climate variability is incredibly important for policymakers and stakeholders in California due to its vast agricultural industry, wide demographics, and vulnerability to anthropogenically-induced climate change (Hayhoe et al. 2004; Cayan et al. 2008). Existing studies show that RCMs are able to capture physically consistent regional and local circulations at the needed spatial and time scales (Leung et al. 2003a; Laprise 2008; Rummukainen 2010). RCM simulations over California have also been conducted in previous studies and showed the need of high resolution to better study regional climate and extreme events, especially over complex topography with large climate gradients (Leung et al. 2004; Kanamitsu and Kanamaru 2007; Caldwell et al. 2009; Pan et al. 2011; Pierce et al. 2013). Caldwell et al. (2009), in particular, presented results from WRF (Weather Research and Forecasting) at 12km spatial resolution showing both the overall consistency and some biases between simulations and observations.

This paper is organized as follows. Section 2 describes the model setup, verification data and evaluation methods. In section 3, results are demonstrated focusing on 2 m temperature (Ts) and precipitation (Pr). Key results are summarized along with further discussion in section 4.

## 2. Models and Methodology

### a. Simulation design

All simulations use the AMIP (Atmospheric Model Intercomparison Project) protocols (Gates 1992). AMIP simulations attempt to recreate a climatology similar to that observed over the past few decades. The ocean model is disabled and the model is forced with prescribed sea-surface temperatures (SSTs) and ice concentrations.

<sup>124</sup> 1) VARRES-CESM

<sup>125</sup> CESM is a state-of-the-art Earth modeling framework developed by the National Center for At-  
<sup>126</sup> mospheric Research (NCAR), consisting of atmospheric, oceanic, land and sea ice components  
<sup>127</sup> and has been heavily used for understanding the effects of global climate change (Neale et al.  
<sup>128</sup> 2010a; Hurrell et al. 2013). Different component models are connected by a couple component.  
<sup>129</sup> In this way, the interfacial states and fluxes between the various component models are commu-  
<sup>130</sup> nicated and the fluxed quantities are conserved. Since we follow AMIP protocols in this study,  
<sup>131</sup> communication is mainly occurred between atmospheric and land model. Ocean model and sean  
<sup>132</sup> ice component are disabled. Here, CAM version 5 (CAM5) (Neale et al. 2010b) and the Com-  
<sup>133</sup> munity Land Model (CLM) version 4 (Oleson et al. 2010) are used. As mentioned earlier, SE  
<sup>134</sup> was used as the dynamical core in CAM along with the variable-resolution grid support. The  
<sup>135</sup> FAMIPC5 (F\_AMIP\_CAM5) compset was chosen for the simulations as it is the standard protocol  
<sup>136</sup> for AMIP and is less computationally demanding.

<sup>137</sup> For our study, the variable-resolution cubed-sphere grids are generated for use in CAM and CLM  
<sup>138</sup> with the open-source software package SQuadGen (Ullrich 2014). The grids used are depicted in  
<sup>139</sup> Figure 2. The maximum horizontal resolution on these grids are 0.25 degree ( $\sim 28\text{km}$ ) and 0.125  
<sup>140</sup> degree ( $\sim 14\text{km}$ ), with a 1 degree resolution covering the rest of the globe. These resolutions  
<sup>141</sup> have been selected because CAM-SE naturally supports a 2:1 aspect ratio, meaning there are two  
<sup>142</sup> transition layers from 1 degree to 0.25 degree, and one additional transition from 0.25 degree to  
<sup>143</sup> 0.125 degree. The meteorological patterns (e.g. wind, pressure and precipitation) showed natural  
<sup>144</sup> and conserved results over the transition boundary as described in (Zarzycki et al. 2015). The time  
<sup>145</sup> period is from 1979-01-01 to 2005-12-31 (UTC), and year 1979 was discarded as spin up time for  
<sup>146</sup> CLM4.0. We chose this time period to present the recent historical climate and try to achieve the

<sup>147</sup> best balance between reproducibility and computational feasibility, which is further discussed in  
<sup>148</sup> the Methodology part.

<sup>149</sup> Variable-resolution topography files have been produced by starting with the National Geophys-  
<sup>150</sup> ical Data Center (NGDC) 2-min ( $\sim 3.5$  km) Gridded Global Relief Dataset (ETOPO2v2) topog-  
<sup>151</sup> raphy dataset and applying the differential smoothing technique by adjusting the c parameter from  
<sup>152</sup> Eq. (1) in Zarzycki et al. (2015). Land surface datasets, and plant functional types, were created at  
<sup>153</sup> the standard 0.50 degree resolution. Greenhouse gas (GHG) concentrations are prescribed based  
<sup>154</sup> on historical observations. SSTs and ice coverage are supplied by the 1degree Hadley Centre Sea  
<sup>155</sup> Ice and Sea Surface Temperature dataset (HadISST) (Hurrell et al. 2008). Tuning parameters are  
<sup>156</sup> not modified from their default configuration.

## <sup>157</sup> 2) UNIFORM CESM

<sup>158</sup> Output from a globally uniform CESM run at  $0.25^\circ$  global spatial resolution is utilized for com-  
<sup>159</sup> parison. It helps us to see if variable-resolution CESM, which is at much lower computation cost  
<sup>160</sup> than uniform one, can show comparable performance in modeling mean climatology (Bacmeister  
<sup>161</sup> et al. 2014). This globally uniform simulation uses the CAM5-FV (finite volume) dynamical core  
<sup>162</sup> and is described in additional detail in Wehner et al. (2014a) and Wehner et al. (2014b). Note that  
<sup>163</sup> the appendix of the latter paper lists parameters that are different from the public release. **need to**  
<sup>164</sup> **add details about this and which parameters are different from the public version.**

## <sup>165</sup> 3) WRF

<sup>166</sup> WRF has gained wide acceptance in studying regional climate over the past decade, showing  
<sup>167</sup> its adequate capability in representation of fine-scale climate properties (Lo et al. 2008; Leung  
<sup>168</sup> and Qian 2009; Soares et al. 2012). In this study, the fully compressible non-hydrostatic WRF

model in version 3.5.1 with the Advanced Research WRF (ARW) dynamical solver is used. ERA (ECMWF re-analysis)-Interim surface and pressure-level reanalysis was used to provide initial and lateral conditions for the domains. The lateral conditions and SSTs were updated every 6 hours. ERA-Interim reanalysis ( $\sim$ 80 km) has been widely used and validated for its reliability as forcing data (Dee et al. 2011). Two simulations are conducted with horizontal resolution of 27km and 9km simultaneously, over the time period 1979-01-01 to 2005-12-31 (UTC). The year 1979 is used as a spin-up period and is discarded for purposes of analysis. The  $\sim$ 10 km resolution is actually finer than most previous studies for long-term climate.

The simulation domains of WRF 9km are depicted in Figure 1. For the WRF 27km simulation, one domain is used. For the WRF 9km simulation, two nested domains are used with the outer domain at 27km (same as the WRF 27km) and inner domain at 9km horizontal grid resolution. As a common way in WRF, two-way nesting is enabled by feeding back information from the fine grid onto the coarse grid, thus the nested region's process of the coarse domain is replaced by the fine grid result (Skamarock and Klemp 2008). These choices have been made to satisfy the natural WRF refinement ratio of 3:1. Both grids are centered on CA and have respectively,  $120 \times 110$  and  $151 \times 172$  grid points. Around the boundaries, 10 grid points are used as lateral relaxation zones. In order to reduce the drift between forcing data and RCM, grid nudging (Stauffer and Seaman 1990) was applied to the outer domain every 6 hours at all levels except the planetary boundary layer (PBL) as suggested by Lo et al. (2008). This setup uses 41 vertical levels with model top pressure at 50 hPa. The topography data used in 27km and 9km are interpolated from USGS (U.S. Geological Survey) elevation data with 10m and 2m resolution respectively.

Additionally, we used the following physics parameterizations: WSM (WRF Single-Moment) 6-class graupel microphysics scheme (Hong and Lim 2006), Kain-Fritsch cumulus scheme (Kain 2004), CAM shortwave and longwave radiation schemes (Collins et al. 2004). These settings

193 are supported by the one-year test running result with different options of cumulus scheme and  
194 radiation schemes. For the boundary layer, the Yonsei University scheme (YSU) (Hong et al.  
195 2006) and the Noah Land Surface Model (Chen and Dudhia 2001) were used. Both were chosen  
196 as they are common for climate applications that balance long-term reliability and computational  
197 cost.

198 *b. Topography*

199 The grid-scale topography for all simulations is contrasted in Figure 3. The higher resolution  
200 simulations provide a much finer representation of regional topography. This is important for  
201 understanding local climate since topography is an important driver for fine-scale dynamic pro-  
202 cesses, especially over complex terrain. Some differences are also apparent between the 28km  
203 varres-CESM and 27km WRF model, particularly over the Central Valley, and indicative of a  
204 different methodology for preparation of the topography dataset.

205 *c. Datasets*

206 For validation purpose, available reanalysis and gridded observational datasets of the highest  
207 quality are employed (see Table 1). These data products incorporate station measurements or  
208 satellite information and other data. Although these products are generally based on observations,  
209 they are based on different network of weather stations. And these datasets are scaled and gridded  
210 using varied interpolation techniques, elevation model and processing algorithms. In this way,  
211 using more reference datasets rather than one is important to account for the uncertainties, for  
212 assessing the performance of the WRF and CESM simulations in terms of both mean behavior  
213 and variability. Moreover, in this study, our purpose of using these products is to serve as realistic  
214 proxies to allow for a comparison of the model results. We acknowledge that reanalysis products

215 are particularly sensitive to model choice and choice of assimilated observations and so cannot be  
216 treated as truth. Detailed descriptions of these datasets are as follows.

217 (i) *NARR*: The North American Regional Reanalysis (NARR) (Mesinger et al. 2006) provides  
218 dynamically downscaled data over North America at  $\sim 32$  km resolution and 3 hourly intervals  
219 from 1979 through present. It is National Centers for Environmental Prediction (NCEP)'s high  
220 resolution reanalysis product combined model and assimilated dataset. All major climatological  
221 variables are present in NARR, making it an excellent candidate for assessment of regional cli-  
222 mate. Nonetheless, some inaccuracies have been identified in NARR that must be accounted for,  
223 including deficiencies in precipitation fields away from the continental US (Bukovsky and Karoly  
224 2007).

225 (ii) *NCEP CPC*: This data set is CPC unified gauge-based analysis of daily precipitation pro-  
226 vided by the National Oceanic and Atmospheric Administration (NOAA) Climate Prediction Cen-  
227 ter (CPC). It is a suite of unified precipitation products with consistent and improved quality by  
228 combining all information available at CPC and by taking advantage of the optimal interpolation  
229 (OI) objective analysis technique. The gauge analysis covers the Conterminous United States on  
230 a fine-resolution at  $0.25^\circ$  from 1948/01/01 to 2006/12/3.

231 (iii) *UW*: The UW daily gridded meteorological data is obtained from the Surface Water Mod-  
232 eling group at the University of Washington (Maurer et al. 2002; Hamlet and Lettenmaier 2005).  
233 UW incorporated topographic corrections by forcing the long-term average precipitation to match  
234 that of the PRISM dataset. Temperature dataset is produced in a similar fashion as precipitation,  
235 but used a simple  $6.1$  K/km lapse rate for topographic effect. The dataset is at  $0.125^\circ$  horizontal  
236 resolution and provided from year 1949 to 2010.

237 (iv) *PRISM*: The Parameter-elevation Regressions on Independent Slopes Model (PRISM) (Daly  
238 et al. 2008) supports a 4km gridded dataset obtained by taking wide range of point measurements  
239 and applying a weighted regression scheme that accounts for many factors affecting the local cli-  
240 matology. The datasets include total precipitation and minimum/maximum, (derived) mean tem-  
241 peratures and dewpoints, based on sophisticated quality control measures. Monthly climatological  
242 variables are available for 1895 through 2014 provided by the PRISM Climate Group. PRISM is  
243 U.S. Department of Agriculture (USDA)'s official climatological data. We will use this product as  
244 the main reference dataset for model assessment.

245 (v) *Daymet*: Daymet is an extremely high resolution (1 km) gridded dataset with daily outputs  
246 of total precipitation, humidity, and minimum/maximum temperature covering the years of 1980  
247 through 2013 (Thornton et al. 1997; Thornton and Running 1999; Thornton et al. 2000). The  
248 dataset is produced using an algorithmic technique that ingests point station measurements in  
249 conjunction with a truncated Gaussian weighting filter. Some adjustments are made to account for  
250 topography. Daymet is available through the Oak Ridge National Laboratory Distributed Active  
251 Archive Center (ORNL DAAC).

252 *d. Methodology*

253 We have analyzed both the near surface (2 meter) temperature and precipitation over California,  
254 in order to assess the models' performances in representing the mean climatology. Specifically,  
255 evaluation will focus on daily maximum, minimum and average 2m temperatures (Tmax, Tmin  
256 and Tavg), and daily precipitation (Pr). These variables are key for a baseline climate assessment,  
257 particularly for their relationship with water resources, agriculture and health. With the overall  
258 warm climate and large impact of heat waves over CA, we will focus on the summer season over  
259 June, July and August (JJA) in the aspect of temperature. Since the vast majority of precipitation

260 in CA occurs in the winter season, together with the accumulation of snowpack, in this way,  
261 precipitation over December-January-February (DJF) will be emphasized. Those seasons also  
262 represent the most part of the climate variability.

263 In order to adequately account for natural variability even regionally, simulations need to be  
264 run long enough (Solomon 2007). However, there is no particular timeframe for climatology  
265 studies. Average weather conditions over 30-year or so are typically used to track climate to make  
266 sure that the data is long enough to calculate an average that is not influenced by year-to-year  
267 variability (Dinse 2009). In this study, 26-year current-climate runtime is chosen to reasonably  
268 balance the reproducibility and computational availability. We have studied the variability of mean  
269 temperature and precipitation in both simulations and observations over 5, 10, 20 and 25 seasons  
270 or years, and the results showed that 20 or 25 years' simulation are long enough to adequately  
271 capture the regionally climate variability. 30 years or longer run time may sound better, but are  
272 not necessary for our case.

273 All the results showed in the following part are based on the time period year 1980 to 2005. All  
274 the datasets have been investigated first to see if time trend exists over this 26 years period, and  
275 the least squares linear trend has been removed from original datasets if existing. It is found that  
276 for temperature, there do exist statistically significant linear trend over some parts of CA under the  
277 two-tailed t-statistic significance level of 0.05. However, no significant trend has been detected for  
278 precipitation.

279 Further, in order to better assess the treatment of California's varied climate regions, the state  
280 has been divided into five regional zones, including: the Central Valley, Mountain Region, North  
281 Coast, South Coast, and Desert Region (Figure 1). The division of these five zones are loosely  
282 based on the results of Abatzoglou et als study (Abatzoglou et al. 2009) and the building climates  
283 zones from California Energy Commission. For parts of the results analyses, simulations and

284 datasets are masked to restrict climate variables to specific zones. We aim to examine the statistics  
285 of data averaged over geographic climate zones instead of just on grid-cell analysis.

286 Some statistical measurements have been used to quantify the performances of the models com-  
287 paring with the reference datasets. These statistical variables include the Root-mean-square devia-  
288 tion (RMSD), mean absolute difference (MAD), mean relative difference (MRD) and correlation,  
289 and sample standard deviation.

290 When calculating the difference at grid point, the reference datasets are remapped to the given  
291 model's output resolution. Datasets are remapped using a bilinear interpolation method, which  
292 has been verified to provide satisfactory performance. Other remapping algorithms, such as patch-  
293 based have been tested and do not exhibit notable differences.

294 Student's t-test is used when necessary to see if two sets of yearly or seasonally averaged data are  
295 significantly different from each other, and 0.05 is used as critical levels of significance. We need  
296 to point out that this is just a approximate test to further support our results analysis since the two  
297 populations being compared should follow a normal distribution.

### 298 **3. Results**

#### 299 *a. Temperature*

300 The mean JJA Tmax, Tmin and Tavg climatology over 26 years are shown in Figure 4. And the  
301 statistical measurements over whole CA area are showed in Table 2. All simulations captured the  
302 spatial climate patterns showed by the PRISM, with high spatial correlations ( $>0.95$ ), especially  
303 for Tmax and Tavg. For Tmax, comparing reference datasets, CESM simulations showed warmer  
304 climate generally, especially uniform CESM. However, WRF output displayed overall colder cli-

305 mate, especially the WRF 9km. Tmax overall Central Valley has been overestimated by all the  
306 simulations.

307 For Tmin, varres-CESM showed a larger warm effect, with a particularly egregious overestima-  
308 tion of Tmin over Nevada (although difference are much smaller when focusing exclusively on  
309 California). Comparing with reference datasets, WRF had better performance than varres-CESM  
310 with smaller differences, especially for WRF 9km. However, the pattern of Tmin present in Figure  
311 4 in both WRF simulations suggests a cooler interior to the Central Valley and warmer perimeter,  
312 which is not supported by observations. Overestimation of Tmin by varres-CESM leads a similar  
313 overestimation for Tavg. And underestimation of Tmax by WRF, causes a underestimation for  
314 Tavg, but still statistically more close to reference datasets than CESMs. The sample standard de-  
315 viation of the JJA Tmax, Tmin and Tavg by models and PRISM are showed in Figure 5. It can be  
316 seen that the variability has little changes across difference sub-zones, and the values are around  
317 0.5 to 1.5 °Cfor all the datasets, except some higher values over mountains regions in WRF 9km.

318 The RMSD values between the models and reference datasets range from ~2 to 4°C. We have  
319 made the Student's t-test to test the if the mean temperature climatology from PRISM, UW and  
320 Daymet are statistically different from each other. And the results we got is that they are the same  
321 at the significance level of 0.05 over most regions of our study area, except coastal regions. There  
322 are some minor uncertainties, as we already discussed, showed when comparing with different  
323 reference datasets. However, it can still be seen that varres-CESM is comparable to WRF and  
324 uniform CESM, without meaning that they are statistically the same. Overall, varres-CESM 0.125  
325 degree performed better in simulating long-term Tmax, WRF is better at modeling Tmin than  
326 varres-CESM. Varres-CESM overestimated all JJA temperatures (especially Tmin), whereas WRF  
327 underestimates Tmax and Tavg. When comparing against NARR (not showed), the overestimation  
328 of Tmin are largely reduced for varres-CESM. This suggests that the source of the temperature

329 bias in varres-CESM and NARR may be related. Also, there are a positive 2 K SST bias near  
330 the California coastline, when comparing varres-CESM and WRF simulations. This may cause  
331 overestimation of temperatures.

332 This is especially encouraging since differences in the varres-CESM simulations, which only  
333 used prescribed SSTs, closely matched those of WRF, which were also forced at the lateral domain  
334 boundaries with reanalysis data. Differences between the reference datasets is relatively smaller  
335 than between the models and reference datasets, thus uncertainties are unlikely impacting the  
336 evaluation results. Also, the sea breeze effect, associated with cooler temperatures near the San  
337 Francisco Bay, are apparent in all runs.

338 The seasonal cycle of Tavg is shown in Figure 6 for simulations and reference data from PRISM  
339 and NARR. The models do show good consistency with reference data with no larger than a 2°C  
340 difference, which mainly occurred in the coldest and hottest seasons. Compared with PRISM,  
341 Varres-CESM showed positive difference over the summer season in all sub-zones except coastal  
342 regions, and negative difference over winter season in all zones. The uniform CESM is similar to  
343 varres-CESM, with larger difference. WRF showed better performance in presenting the monthly  
344 trend than CESM with a little underestimation over all seasons. No notable differences can be  
345 discerned when comparing models across resolutions.

346 The variability over each month is expressed by the sample standard deviation showed in Figure  
347 7. Generally, local variability of Tavg is under the magnitude of 3°C, mostly within the range  
348 from 1 to 2°C. Among the simulations, WRF 27km is most consistent with PRISM. WRF 9km  
349 is also close to PRISM, but has ~1°C larger variability over January and February. Varres-CESM  
350 basically showed about 0.5°C more scattered values (either above or lower) comparing to reference  
351 datasets, and uniform CESM has a about 0.5°C lower variability than others.

352 For the temperature climatology in California, we are most interested in the Tmax over summer  
353 season due to the impact of summer heat extremes. We depict the frequency distribution of Tmax  
354 using all the JJA daily values over 26 years. The results of the simulations and reference datasets  
355 including Daymet and UW are showed in Figure 8. Properties of the Frequency distribution, in-  
356 cluding average, variability, skewness and Kurtosis are tabulated in Table 3. Though with some  
357 deviations, similar distribution shapes with tails off to left are present for both models and obser-  
358 vations. Contrasting with WRF, varres-CESMs are more close to reference datasets. WRF 9km  
359 tended to be colder. Models including varres-CESM and WRF 27km are more consistent with  
360 observations for higher values than the peak and less consistent at lower values. For representa-  
361 tion of heat extremes, both varres-CESM and WRF 27km exhibit satisfactory performance over  
362 most regions except in Central Valley (CV). No obvious improvement is associated with higher  
363 resolution in varres-CESM.

364 In the CV, the models show a clear warm effect and associated long tail, with temperatures  
365 reaching near 50°C. As discussed before, all models do overestimate Tmax in the CV. In order to  
366 further assess the accuracy of the gridded observations, we examine the Tmax data directly from  
367 recorded weather station observations over the CV. The results validate that Tmax values above  
368 45°C are rare (although station observations suggest these days may be slightly more frequent  
369 than suggested by UW and Daymet). The warm bias associated with the aforementioned extreme  
370 hot days in both varres-CESM and WRF is likely due to reasons discussed in Caldwell et al.  
371 (2009) where biases were correlated with overly dry summertime soil moisture. This could be  
372 caused by the lack of accurate land surface treatment in climate models. areas. Bonfils and Lobell  
373 (2007) found that irrigation in California's Central Valley has significantly decreased summertime  
374 maximum temperatures especially in heavily-irrigated areas (Bonfils and Lobell 2007). Other

<sup>375</sup> studies can also be found for the cooling climatic effects of irrigation, such as (Kueppers et al.  
<sup>376</sup> 2007).

<sup>377</sup> *b. Precipitation*

<sup>378</sup> California is known for the shortage of natural water resources with extreme drought over sum-  
<sup>379</sup> mer season. Instead, the winter season is particularly important for California as it accounts for 50  
<sup>380</sup> percent of the 22.5 inches that California receives for its total annual average precipitation amounts  
<sup>381</sup> (<http://www.ncdc.noaa.gov/cag/>).

<sup>382</sup> The long-term average climatologies of DJF and annual daily precipitation (Pr) over 26 years  
<sup>383</sup> from simulations and reference datasets are displayed in Figure 9. And the statistical measure-  
<sup>384</sup> ments over whole CA area are showed in Table 4. As we can see, precipitation is distributed  
<sup>385</sup> mostly along the North coast and Sierra Nevada mountains, and is relatively sparse in other re-  
<sup>386</sup> gions. As temperature, simulations also captured the spatial patterns of the PRISM, with high  
<sup>387</sup> correlation coefficients (>0.94). However, there does exist clear differences among simulations.

<sup>388</sup> Varres-CESM overestimates total precipitation, especially in the coarse resolution (28 km) sim-  
<sup>389</sup> ulation (about 40%-50%) along the western side of Sierra Nevada resulting statistical difference  
<sup>390</sup> over this area comparing with PRISM. The finer resolution simulation produces a slight reduction  
<sup>391</sup> of difference with magnitude near 1 mm/day, likely due to improved treatment of orographic ef-  
<sup>392</sup> fects as showed in Figure 3. Interestingly, varres-CESM 0.125° is statistically the same as PRISM.  
<sup>393</sup> Uniform CESM has slighter better results than varres-CESM 0.25deg. Notably, there are large dif-  
<sup>394</sup> ferences between WRF 27km and WRF 9km. WRF 27km underestimates precipitation slightly  
<sup>395</sup> (about 30%), whereas WRF 9km shows a large positive difference (about 70%-80%) along the  
<sup>396</sup> North coast and the Sierra Nevada of up to 50 percent. However, WRF 9km and WRF 27km are  
<sup>397</sup> both significantly the same at the significance level of 0.05 as PRISM except the mountain region,

398 considering the variability within them as showed in the Figure 10. From the sample standard  
399 deviation of the precipitation displayed in Figure 10, we can see that the variability has similar  
400 patterns of the precipitation intensity distribution, and increases as the precipitation magnitude  
401 increases. Models seems capture the variation of precipitation well except the 50% higher values  
402 of WRF 9km, and the varres-CESM 0.125deg and WRF 27 km showed more realistic values than  
403 others comparing with PRISM.

404 The reference datasets also have notable differences indicating uncertainty inherent in interpo-  
405 lating station data to a grid. However, these observations are still of the highest quality available  
406 and the uncertainty is relatively small compared with difference from the simulations. We have  
407 also made the Student's t-test to test the if the mean precipitation climatology from PRISM, UW  
408 and Daymet are statistically different from each other. And the results we got is that they are al-  
409 most the same at the significance level of 0.05 over all the study area. Therefore, the uncertainties  
410 within them are negligible. Overall, varres-CESM  $0.125^\circ$  performs slightly better than CESM  
411  $0.25^\circ$  and WRF 27km, as further exhibited by the RMSD values in Table 4.

412 The climatological annual cycle of precipitation averaged over each sub-region is presented in  
413 Figure 11. It can be seen that simulations showed similar trend as reference datasets. The main  
414 deviation occurred during the rainy seasons, especially in winter. WRF 27km is drier in all regions  
415 and WRF 9km is far wetter in all regions. Varres-CESM tracks well with observed precipitation  
416 everywhere except in the Central Valley, where precipitation is overestimated. Nonetheless, the  
417 strong seasonal dependence on precipitation is apparent in all regions with extremely dry condi-  
418 tions during summer months. A slight increase in summertime precipitation is apparent in the  
419 Desert region, indicating the North American monsoon. Overall, varres-CESM is more consis-  
420 tent with observations in most regions and in all seasons compared with WRF. However, we also  
421 observe that the peak month for precipitation tends to occur earlier in varres-CESM than in obser-

vations. It is not surprising that a seasonal time drift occurred with the varres-CESM simulations as it was not forced by a reanalysis dataset (unlike the WRF simulations).

The variability over each month is expressed by the sample standard deviation showed in Figure 12. It can be seen that variability has similar monthly trend as the annual cycle of precipitation, with overall value from 0 to 4 mm/day, which generally shows higher interannual variability over locations of higher mean precipitation 11. Varres-CESM also exhibited a slightly larger variability in the rainy season than observations, while WRF 27km showed a little reduced values. WRF 9km showed notable larger variability compared with observations during rainy seasons over most regions. Such higher variability within finer resolution has also been found in previous studies. Duffy et al. (2006) discussed the higher variability caused by higher spatial resolution used in RCM models, allowing more accurate representation of topography, which is likely, at least in part, to be the reason (Duffy et al. 2006). The main cause of the interannual variability of precipitation over CA is El NioSouthern Oscillation (ENSO), which varies the amount of moisture flux transported to this region.

The frequency distribution of DJF Pr has been constructed from rainy days in winter ( $\text{Pr} \geq 0.1 \text{mm/d}$ ) and depicted in Figure 13. It can be seen that varres-CESM is more consistent with observations everywhere except in the CV. In this region WRF 27km appears to better capture high-intensity precipitation events, but performs more poorly on low-intensity events. The underestimation of rainfall frequency in WRF 27km appears consistent across regions. WRF 9km produces a significantly better treatment of low-intensity events, but greatly overestimates the frequency of high-intensity events. Notably, varres-CESM 0.25 degree and varres-CESM 0.125 degree do not show significant differences. For strong precipitation events, varres-CESM and WRF 27km show good performance over most regions except in those noted above, although these conclusions are also constrained by observational uncertainty.

446 The positive deviation of precipitation using WRF at high resolution has also been found in  
447 former studies. Caldwell et al. (2009) also showed that WRF at 12km largely overestimate the  
448 precipitation over the mountain division of CA. The deviation magnitude is less than what showed  
449 in this study due to different division area and different setting of microphysics. In Caldwell's  
450 paper aforementioned, possible reasons have been discussed in detail, stating a variety of source  
451 including the model itself and the choice of physical parameterizations. A comprehensive analysis  
452 of the cause of these errors is beyond the scope of this paper. Further discussion can be found  
453 in former studies including the use of different microphysics schemes and resulting change of  
454 precipitation magnitude (Leung et al. 2003b; Jankov et al. 2005; Gallus Jr and Bresch 2006; Chin  
455 et al. 2010; Caldwell 2010).

456 Finally, a concise summary of model performance over CA is provided by the Taylor diagram  
457 (Figure 14). This diagram includes the spatial centered correlation between the simulated and  
458 observed fields, the RMS variability of simulations normalized by that in the observations, and  
459 mean differences from reference data. It can be seen that the models correlate well with the PRISM  
460 reference dataset. Normalized standard deviation and bias are larger for precipitation, especially  
461 for WRF 9km. Overall, varres-CESM has demonstrated that it can competitively compare to WRF  
462 in capturing the regional climatology of California. ([update the plot](#))

#### 463 **4. Discussions and summary**

464 This study has evaluated the performance of a relatively new variable-resolution GCM model,  
465 i.e. varres-CESM in simulating California climatology for regional climate studies. This new tech-  
466 nique is studied against WRF as a traditional RCM. Gridded datasets are used to help us evaluate  
467 the modeling results. As the need for assessments of regional climate change is increasing, alter-  
468 native modeling strategies, including variable-resolution global climate models will be needed to

469 improve our understanding of the effects of fine-scale processes representation in regional climate  
470 regulation.

471 Based on 26 years of high-resolution historical climate simulations, we analyzed both tempera-  
472 ture and precipitation in California and across its climate divisions. We found that varres-CESM  
473 output have comparable performance as WRF for mean climatology, although the model still pos-  
474 sessed a slight tendency to a warmer and moister climate, especially in the Central Valley which  
475 is surrounded by mountain and coastal region. WRF exhibited a clear colder summer Tmax over  
476 most regions except the Central Valley, but a little warmer in summer Tmin. Varres-CESM showed  
477 better ability in reproducing Tmax, however, looking at the magnitude of statistical measurements,  
478 WRF was better at modeling Tmin and Tavg. WRF presents the monthly trend better than CESM  
479 with a little underestimation over all seasons, with smaller temperature range.

480 For representation of heat extremes, both varres-CESM and WRF 27km exhibit satisfactory  
481 performance over most regions except in Central Valley (CV). This is likely caused by the loss  
482 of irrigation cooling effect over this region and irrigation effect is rarely considered in long-term  
483 climate modeling. In future work, we will add irrigation effect in varres-CESM to figure out the  
484 role irrigation played in regulating Tmax, to reduce the overestimation and longer upbounded tail  
485 of frequency distribution for Tmax,

486 The main precipitation modeling deviations occurred during rainy seasons, especially in win-  
487 ter. Varres-CESM overestimates precipitation especially along the western side of Sierra Nevada,  
488 though the finer resolution simulation produces a slight reduction likely due to improved treatment  
489 of orographic effects. WRF 27km underestimates precipitation slightly, whereas WRF 9km shows  
490 a large overestimation. It can be seen that simulations showed similar seasonal trend as refer-  
491 ence datasets, with main deviation occurred during the rainy seasons. Varres-CESM also exhibited  
492 a slightly larger variability than WRF 27km. For strong precipitation events, varres-CESM and

493 WRF 27km show satisfactory modeling ability over most regions (except the Central Valley, in the  
494 case of varres-CESM), although the reference datasets also show some uncertainties.

495 Higher resolution ( $0.125^{\circ}$ ) simulations with varres-CESM were quite similar to the coarser reso-  
496 lution runs, although there were not too significant improvements in capturing summer Tmax and  
497 precipitation, and their corresponding variability. For WRF, simulation at finer resolution (9km)  
498 also did not really show meaningful improvement in representing finer regional climatology. When  
499 resolution increased, WRF produce a obviously overestimated precipitation over the North coastal  
500 region and the mountain region. This is not surprising since previous studies have also found  
501 this phenomenon for fine-scale simulations using RCMs as aforementioned. The use convection  
502 scheme is perhaps not needed when grid spacing is near 10km. However, it turned out that almost  
503 all of the precipitation comes from resolved (large-scale) processes for all these models. In this  
504 way, model deviation is mainly related with resolved-scale processes and microphysics scheme  
505 plays a major role, which makes it necessary to develop more scale-aware parameterizations.

506 The importance and necessity of high resolution for regional climate studies has been widely  
507 stressed by previous studies. However, whether the current regional climate models can fulfill this  
508 demand when resolution is pushed to local scales is questionable. It is clear that further work is  
509 urgently needed to solve the scale limitation of current regional climate models at fine horizontal  
510 resolutions. The possible causes of the scale limitation may include a lack of accurate scale-aware  
511 physical parameterizations near or below 10 km horizontal resolution, the treatment of dynamics  
512 at fine scales, and the interactions among different components of RCMs or VR-GCMs (e.g., land-  
513 atmosphere interactions).

514 Generally, when compared with reference datasets, simulations do a good job of capturing re-  
515 gional climatological patterns with high spatial correlations. Deviations are not indicative of deep  
516 underlying problems with the model formulation, but one should be aware of these differences

517 when using these models for assessing future climate change. Uncertainty between observational  
518 datasets exists, but is relatively small. Compared with the uniform resolution CESM-FV sim-  
519 ulation, varres-CESM performed similarly or even a little better in some cases, which gives us  
520 more confidence to use this technique in further climate change studies. In summary, varres-  
521 CESM demonstrated competitive utility for studying high-resolution regional climatology when  
522 compared to a regional climate model (WRF) and a uniform high-resolution GCM (CESM-FV).  
523 This study suggests that variable-resolution GCMs are useful tools for assessing climate change  
524 over the coming century.

525 *Acknowledgments.* The authors would like to thank Michael Wehner and Daíthí Stone for pro-  
526 viding the uniform resolution CESM dataset. We would further like to thank Travis O'Brien for  
527 his many useful conversations on climate model assessment. We also want to thank Xuemeng  
528 Chen for her assistance in WRF running. This project is supported in part by the University of  
529 California, Davis and by the Department of Energy “Multiscale Methods for Accurate, Efficient,  
530 and Scale-Aware Models of the Earth System” program.

## 531 References

- 532 Abatzoglou, J. T., K. T. Redmond, and L. M. Edwards, 2009: Classification of regional climate  
533 variability in the state of California. *Journal of Applied Meteorology and Climatology*, **48** (8),  
534 1527–1541.
- 535 Bacmeister, J. T., M. F. Wehner, R. B. Neale, A. Gettelman, C. Hannay, P. H. Lauritzen, J. M.  
536 Caron, and J. E. Truesdale, 2014: Exploratory high-resolution climate simulations using the  
537 Community Atmosphere Model (CAM). *Journal of Climate*, **27** (9), 3073–3099.

- 538 Bonfils, C., and D. Lobell, 2007: Empirical evidence for a recent slowdown in irrigation-induced  
539 cooling. *Proceedings of the National Academy of Sciences*, **104** (34), 13 582–13 587.
- 540 Bukovsky, M. S., and D. J. Karoly, 2007: A brief evaluation of precipitation from the North  
541 American Regional Reanalysis. *Journal of Hydrometeorology*, **8** (4), 837–846.
- 542 Bukovsky, M. S., and D. J. Karoly, 2009: Precipitation simulations using WRF as a nested regional  
543 climate model. *Journal of Applied Meteorology and Climatology*, **48** (10), 2152–2159.
- 544 Caldwell, P., 2010: California wintertime precipitation bias in regional and global climate models.  
545 *Journal of Applied Meteorology and Climatology*, **49** (10), 2147–2158.
- 546 Caldwell, P., H.-N. S. Chin, D. C. Bader, and G. Bala, 2009: Evaluation of a WRF dynamical  
547 downscaling simulation over California. *Climatic Change*, **95** (3-4), 499–521.
- 548 Cayan, D. R., A. L. Luers, G. Franco, M. Hanemann, B. Croes, and E. Vine, 2008: Overview of  
549 the California climate change scenarios project. *Climatic Change*, **87** (1), 1–6.
- 550 Chen, F., and J. Dudhia, 2001: Coupling an advanced land surface-hydrology model with the Penn  
551 State-NCAR MM5 modeling system. Part I: Model implementation and sensitivity. *Monthly  
552 Weather Review*, **129** (4), 569–585.
- 553 Chin, H.-N. S., P. M. Caldwell, and D. C. Bader, 2010: Preliminary study of California wintertime  
554 model wet bias. *Monthly Weather Review*, **138** (9), 3556–3571.
- 555 Christensen, J. H., and Coauthors, 2007: Regional climate projections. *Climate Change, 2007:*  
556 *The Physical Science Basis. Contribution of Working group I to the Fourth Assessment Report  
557 of the Intergovernmental Panel on Climate Change, University Press, Cambridge, Chapter 11,*  
558 847–940.

- 559 Collins, W. D., and Coauthors, 2004: Description of the NCAR community atmosphere model  
560 (CAM 3.0). Tech. rep., Tech. Rep. NCAR/TN-464+ STR.
- 561 Daly, C., M. Halbleib, J. I. Smith, W. P. Gibson, M. K. Doggett, G. H. Taylor, J. Curtis, and P. P.  
562 Pasteris, 2008: Physiographically sensitive mapping of climatological temperature and precip-  
563 itation across the conterminous United States. *International Journal of Climatology*, **28** (15),  
564 2031–2064.
- 565 Dee, D., and Coauthors, 2011: The ERA-Interim reanalysis: Configuration and performance of  
566 the data assimilation system. *Quarterly Journal of the Royal Meteorological Society*, **137** (656),  
567 553–597.
- 568 Dinse, K., 2009: Climate variability and climate change: what is the difference. *Book Climate  
569 Variability and Climate Change: What is the Difference.*
- 570 Duffy, P., and Coauthors, 2006: Simulations of present and future climates in the western United  
571 States with four nested regional climate models. *Journal of Climate*, **19** (6), 873–895.
- 572 Fowler, H., S. Blenkinsop, and C. Tebaldi, 2007: Linking climate change modelling to impacts  
573 studies: recent advances in downscaling techniques for hydrological modelling. *International  
574 Journal of Climatology*, **27** (12), 1547–1578.
- 575 Fox-Rabinovitz, M., J. Côté, B. Dugas, M. Déqué, and J. L. McGregor, 2006: Variable resolution  
576 general circulation models: Stretched-grid model intercomparison project (SGMIP). *Journal of  
577 Geophysical Research: Atmospheres (1984–2012)*, **111** (D16).
- 578 Fox-Rabinovitz, M. S., G. L. Stenchikov, M. J. Suarez, and L. L. Takacs, 1997: A finite-  
579 difference GCM dynamical core with a variable-resolution stretched grid. *Monthly Weather  
580 Review*, **125** (11), 2943–2968.

- 581 Fox-Rabinovitz, M. S., G. L. Stenchikov, M. J. Suarez, L. L. Takacs, and R. C. Govindaraju, 2000:  
582 A uniform-and variable-resolution stretched-grid GCM dynamical core with realistic orography.  
583 *Monthly Weather Review*, **128** (6), 1883–1898.
- 584 Fox-Rabinovitz, M. S., L. L. Takacs, R. C. Govindaraju, and M. J. Suarez, 2001: A variable-  
585 resolution stretched-grid general circulation model: Regional climate simulation. *Monthly*  
586 *Weather Review*, **129** (3), 453–469.
- 587 Gallus Jr, W. A., and J. F. Bresch, 2006: Comparison of impacts of WRF dynamic core, physics  
588 package, and initial conditions on warm season rainfall forecasts. *Monthly Weather Review*,  
589 **134** (9), 2632–2641.
- 590 Gates, W. L., 1992: AMIP: The Atmospheric Model Intercomparison Project. *Bulletin of the*  
591 *American Meteorological Society*, **73**, 1962–1970.
- 592 Hamlet, A. F., and D. P. Lettenmaier, 2005: Production of Temporally Consistent Gridded Precipi-  
593 tation and Temperature Fields for the Continental United States\*. *Journal of Hydrometeorology*,  
594 **6** (3), 330–336.
- 595 Hayhoe, K., and Coauthors, 2004: Emissions pathways, climate change, and impacts on Califor-  
596 nia. *Proceedings of the National Academy of Sciences of the United States of America*, **101** (34),  
597 12 422–12 427.
- 598 Hong, S.-Y., and J.-O. J. Lim, 2006: The WRF single-moment 6-class microphysics scheme  
599 (WSM6). *Asia-Pacific Journal of Atmospheric Sciences*, **42** (2), 129–151.
- 600 Hong, S.-Y., Y. Noh, and J. Dudhia, 2006: A new vertical diffusion package with an explicit  
601 treatment of entrainment processes. *Monthly Weather Review*, **134** (9), 2318–2341.

- 602 Hurrell, J. W., J. J. Hack, D. Shea, J. M. Caron, and J. Rosinski, 2008: A new sea surface temper-  
603 ature and sea ice boundary dataset for the Community Atmosphere Model. *Journal of Climate*,  
604 **21 (19)**, 5145–5153.
- 605 Hurrell, J. W., and Coauthors, 2013: The community earth system model: A framework for col-  
606 laborative research. *Bulletin of the American Meteorological Society*, **94 (9)**, 1339–1360.
- 607 Jankov, I., W. A. Gallus Jr, M. Segal, B. Shaw, and S. E. Koch, 2005: The impact of different WRF  
608 model physical parameterizations and their interactions on warm season MCS rainfall. *Weather*  
609 and Forecasting, **20 (6)**, 1048–1060.
- 610 Kain, J. S., 2004: The Kain-Fritsch convective parameterization: An update. *Journal of Applied*  
611 *Meteorology*, **43 (1)**, 170–181.
- 612 Kanamitsu, M., and H. Kanamaru, 2007: Fifty-seven-year California Reanalysis Downscaling at  
613 10 km (CaRD10). Part I: System detail and validation with observations. *Journal of Climate*,  
614 **20 (22)**, 5553–5571.
- 615 Kueppers, L. M., M. A. Snyder, and L. C. Sloan, 2007: Irrigation cooling effect: Regional climate  
616 forcing by land-use change. *Geophysical Research Letters*, **34 (3)**.
- 617 Laprise, R., 2008: Regional climate modelling. *Journal of Computational Physics*, **227 (7)**, 3641–  
618 3666.
- 619 Laprise, R., and Coauthors, 2008: Challenging some tenets of regional climate modelling. *Meteo-*  
620 *rology and Atmospheric Physics*, **100 (1-4)**, 3–22.
- 621 Leung, L. R., L. O. Mearns, F. Giorgi, and R. L. Wilby, 2003a: Regional climate research: needs  
622 and opportunities. *Bulletin of the American Meteorological Society*, **84 (1)**, 89–95.

623 Leung, L. R., and Y. Qian, 2009: Atmospheric rivers induced heavy precipitation and flooding in  
624 the western US simulated by the WRF regional climate model. *Geophysical research letters*,  
625 **36** (3).

626 Leung, L. R., Y. Qian, and X. Bian, 2003b: Hydroclimate of the western United States based on  
627 observations and regional climate simulation of 1981-2000. Part I: Seasonal statistics. *Journal*  
628 *of Climate*, **16** (12), 1892–1911.

629 Leung, L. R., Y. Qian, X. Bian, W. M. Washington, J. Han, and J. O. Roads, 2004: Mid-century  
630 ensemble regional climate change scenarios for the western United States. *Climatic Change*,  
631 **62** (1-3), 75–113.

632 Lo, J. C.-F., Z.-L. Yang, and R. A. Pielke, 2008: Assessment of three dynamical climate downscal-  
633 ing methods using the Weather Research and Forecasting (WRF) model. *Journal of Geophysical*  
634 *Research: Atmospheres (1984–2012)*, **113** (D9).

635 Maurer, E., A. Wood, J. Adam, D. Lettenmaier, and B. Nijssen, 2002: A long-term hydrologically  
636 based dataset of land surface fluxes and states for the conterminous United States\*. *Journal of*  
637 *climate*, **15** (22), 3237–3251.

638 McDonald, A., 2003: Transparent boundary conditions for the shallow-water equations: testing in  
639 a nested environment. *Monthly Weather Review*, **131** (4), 698–705.

640 Mearns, L. O., and Coauthors, 2012: The North American regional climate change assessment  
641 program: overview of phase I results. *Bulletin of the American Meteorological Society*, **93** (9),  
642 1337–1362.

- 643 Mesinger, F., and K. Veljovic, 2013: Limited area NWP and regional climate modeling: a test  
644 of the relaxation vs Eta lateral boundary conditions. *Meteorology and Atmospheric Physics*,  
645 **119 (1-2)**, 1–16.
- 646 Mesinger, F., and Coauthors, 2006: North American regional reanalysis. *Bulletin of the American*  
647 *Meteorological Society*, **87**, 343–360.
- 648 Neale, R. B., and Coauthors, 2010a: Description of the NCAR community atmosphere model  
649 (CAM 5.0). *NCAR Tech. Note NCAR/TN-486+STR*.
- 650 Neale, R. B., and Coauthors, 2010b: Description of the NCAR Community Atmosphere Model  
651 (CAM 5.0). NCAR Technical Note NCAR/TN-486+STR, National Center for Atmospheric Re-  
652 search, Boulder, Colorado, 268 pp.
- 653 Oleson, K., and Coauthors, 2010: Technical description of version 4.0 of the Community Land  
654 Model (CLM). NCAR Technical Note NCAR/TN-478+STR, National Center for Atmospheric  
655 Research, Boulder, Colorado, 257 pp. doi:10.5065/D6FB50WZ.
- 656 Pan, L.-L., S.-H. Chen, D. Cayan, M.-Y. Lin, Q. Hart, M.-H. Zhang, Y. Liu, and J. Wang, 2011:  
657 Influences of climate change on California and Nevada regions revealed by a high-resolution  
658 dynamical downscaling study. *Climate Dynamics*, **37 (9-10)**, 2005–2020.
- 659 Pierce, D. W., and Coauthors, 2013: Probabilistic estimates of future changes in California temper-  
660 ature and precipitation using statistical and dynamical downscaling. *Climate Dynamics*, **40 (3-**  
661 **4)**, 839–856.
- 662 Rauscher, S. A., E. Coppola, C. Piani, and F. Giorgi, 2010: Resolution effects on regional climate  
663 model simulations of seasonal precipitation over Europe. *Climate Dynamics*, **35 (4)**, 685–711.

- 664 Rauscher, S. A., T. D. Ringler, W. C. Skamarock, and A. A. Mirin, 2013: Exploring a Global  
665 Multiresolution Modeling Approach Using Aquaplanet Simulations. *Journal of Climate*, **26** (8),  
666 2432–2452.
- 667 Rummukainen, M., 2010: State-of-the-art with Regional Climate Models. *Wiley Interdisciplinary*  
668 *Reviews: Climate Change*, **1** (1), 82–96.
- 669 Skamarock, W., J. Klemp, J. Dudhia, D. Gill, and D. Barker, 2005: Coauthors, 2008: A Descrip-  
670 tion of the Advanced Research WRF Version 3. NCAR Technical Note. Tech. rep., NCAR/TN–  
671 475+ STR.
- 672 Skamarock, W. C., and J. B. Klemp, 2008: A time-split nonhydrostatic atmospheric model for  
673 weather research and forecasting applications. *Journal of Computational Physics*, **227** (7),  
674 3465–3485.
- 675 Soares, P. M., R. M. Cardoso, P. M. Miranda, J. de Medeiros, M. Belo-Pereira, and F. Espírito-  
676 Santo, 2012: WRF high resolution dynamical downscaling of ERA-Interim for Portugal. *Cli-*  
677 *mate dynamics*, **39** (9-10), 2497–2522.
- 678 Solomon, S., 2007: *Climate change 2007—the physical science basis: Working group I contribution*  
679 *to the fourth assessment report of the IPCC*, Vol. 4. Cambridge University Press.
- 680 Staniforth, A. N., and H. L. Mitchell, 1978: A variable-resolution finite-element technique for  
681 regional forecasting with the primitive equations. *Monthly Weather Review*, **106** (4), 439–447.
- 682 Stauffer, D. R., and N. L. Seaman, 1990: Use of four-dimensional data assimilation in a limited-  
683 area mesoscale model. Part I: Experiments with synoptic-scale data. *Monthly Weather Review*,  
684 **118** (6), 1250–1277.

- 685 Taylor, M. A., and A. Fournier, 2010: A compatible and conservative spectral element method on  
686 unstructured grids. *Journal of Computational Physics*, **229** (17), 5879–5895.
- 687 Thornton, P. E., H. Hasenauer, and M. A. White, 2000: Simultaneous estimation of daily solar ra-  
688 diation and humidity from observed temperature and precipitation: an application over complex  
689 terrain in Austria. *Agricultural and Forest Meteorology*, **104** (4), 255–271.
- 690 Thornton, P. E., and S. W. Running, 1999: An improved algorithm for estimating incident daily  
691 solar radiation from measurements of temperature, humidity, and precipitation. *Agricultural and*  
692 *Forest Meteorology*, **93** (4), 211–228.
- 693 Thornton, P. E., S. W. Running, and M. A. White, 1997: Generating surfaces of daily meteorolog-  
694 ical variables over large regions of complex terrain. *Journal of Hydrology*, **190** (3), 214–251.
- 695 Ullrich, P. A., 2014: SQuadGen: Spherical Quadrilateral Grid Generator. Accessed: 2015-02-11,  
696 <http://climate.ucdavis.edu/squadgen.php>.
- 697 Warner, T. T., R. A. Peterson, and R. E. Treadon, 1997: A tutorial on lateral boundary conditions  
698 as a basic and potentially serious limitation to regional numerical weather prediction. *Bulletin*  
699 *of the American Meteorological Society*, **78** (11), 2599–2617.
- 700 Wehner, M., Prabhat, K. Reed, D. Stone, W. D. Collins, J. Bacmeister, and A. Gettleman, 2014a:  
701 Resolution dependence of future tropical cyclone projections of CAM5.1 in the US CLIVAR  
702 Hurricane Working Group idealized configurations. *J. Climate*, doi:10.1175/JCLI-D-14-00311.  
703 1, in press.
- 704 Wehner, M. F., and Coauthors, 2014b: The effect of horizontal resolution on simulation qual-  
705 ity in the Community Atmospheric Model, CAM5.1. *J. Model. Earth. Sys.*, doi:10.1002/  
706 2013MS000276.

- 707 Zarzycki, C. M., and C. Jablonowski, 2014: A multidecadal simulation of Atlantic tropical cy-  
708 clones using a variable-resolution global atmospheric general circulation model. *Journal of Ad-*  
709 *vances in Modeling Earth Systems*, **6** (3), 805–828.
- 710 Zarzycki, C. M., C. Jablonowski, and M. A. Taylor, 2014: Using Variable-Resolution Meshes  
711 to Model Tropical Cyclones in the Community Atmosphere Model. *Monthly Weather Review*,  
712 **142** (3), 1221–1239.
- 713 Zarzycki, C. M., C. Jablonowski, D. R. Thatcher, and M. A. Taylor, 2015: Effects of localized  
714 grid refinement on the general circulation and climatology in the community atmosphere model.  
715 *Journal of Climate*, **28** (7), 2777–2803.

## 716 LIST OF TABLES

717	<b>Table 1.</b> Reanalysis and statistically downscaled observational datasets used in this	35
718	study. . . . .	
719	<b>Table 2.</b> RMSD, MAD and Correlation (Corr) for JJA temperature over California . . . . .	36
720	<b>Table 3.</b> The first four moments of the JJA Tmax frequency in each sub-zone. Column	
721	titles refer to Average (Avg), Variance (Var), Skewness (Skew) and Kurtosis	
722	(Kurt). . . . .	37
723	<b>Table 4.</b> RMSD, MAD, MRD, Correlation (Corr) for precipitation over California . . . . .	38

TABLE 1. Reanalysis and statistically downscaled observational datasets used in this study.

<b>Data source</b>	<b>Variables used</b>	<b>Spatial resolution</b>	<b>Temporal resolution</b>
<b>NARR</b>	Pr, $T_s$	32km	daily, 3-hourly
<b>NCEP CPC</b>	Pr	0.125°	daily
<b>UW</b>	Pr, $T_{min}$ , $T_{max}$	0.125°	daily
<b>PRISM</b>	Pr, $T_{min}$ , $T_{max}$ , $T_{avg}$	4km	monthly
<b>Daymet</b>	Pr, $T_{min}$ , $T_{max}$	1km	daily

TABLE 2. RMSD, MAD and Correlation (Corr) for JJA temperature over California

<b>RMSD</b>	<b>UW</b>		<b>PRISM</b>			<b>Daymet</b>	
	$T_{max}$	$T_{min}$	$T_{max}$	$T_{min}$	$T_{avg}$	$T_{max}$	$T_{min}$
<b>varres-CESM 0.25d</b>	2.322	3.745	2.924	3.121	2.604	2.810	3.934
<b>varres-CESM 0.125d</b>	1.900	3.631	2.447	2.944	2.184	2.475	3.701
<b>WRF 27km</b>	2.310	2.738	2.933	2.254	2.169	2.511	2.992
<b>WRF 9km</b>	3.319	2.937	3.492	1.837	1.769	3.203	2.942
<b>uniform CESM 0.25d</b>	3.885	4.088	4.265	3.614	3.536	4.315	4.274
<b>MAD</b>	<b>UW</b>		<b>PRISM</b>			<b>Daymet</b>	
	$T_{max}$	$T_{min}$	$T_{max}$	$T_{min}$	$T_{avg}$	$T_{max}$	$T_{min}$
<b>varres-CESM 0.25d</b>	0.981	2.907	0.606	1.731	0.823	1.177	2.877
<b>varres-CESM 0.125d</b>	0.645	2.848	0.203	1.660	0.579	0.818	2.744
<b>WRF 27km</b>	-0.577	0.819	-0.952	-0.357	-0.771	-0.386	0.789
<b>WRF 9km</b>	-2.277	1.862	-2.720	0.674	-1.142	-2.103	1.757
<b>uniform CESM 0.25d</b>	1.812	2.993	1.449	1.815	1.280	2.013	2.961
<b>Corr</b>	<b>UW</b>		<b>PRISM</b>			<b>Daymet</b>	
	$T_{max}$	$T_{min}$	$T_{max}$	$T_{min}$	$T_{avg}$	$T_{max}$	$T_{min}$
<b>varres-CESM 0.25d</b>	0.998	0.982	0.996	0.986	0.994	0.997	0.979
<b>varres-CESM 0.125d</b>	0.998	0.985	0.997	0.988	0.996	0.997	0.983
<b>WRF 27km</b>	0.997	0.982	0.996	0.989	0.996	0.997	0.978
<b>WRF 9km</b>	0.996	0.985	0.997	0.993	0.998	0.996	0.984
<b>uniform CESM 0.25d</b>	0.994	0.980	0.992	0.981	0.991	0.993	0.977

724 TABLE 3. The first four moments of the JJA Tmax frequency in each sub-zone. Column titles refer to Average  
 725 (Avg), Variance (Var), Skewness (Skew) and Kurtosis (Kurt).

	Central valley				Mountain				North coast				South coast				Desert			
	Avg	Var	Skew	Kurt	Avg	Var	Skew	Kurt	Avg	Var	Skew	Kurt	Avg	Var	Skew	Kurt	Avg	Var	Skew	Kurt
<b>UW</b>	32.6	24.8	-0.8	0.9	26.7	33.2	-0.4	0.3	25.9	30.4	0.1	-0.5	25.9	30.4	0.1	-0.5	37.0	22.9	-0.6	0.7
<b>Daymet</b>	32.7	23.5	-0.9	1.5	25.9	39.3	-0.5	0.5	26.5	30.1	-0.3	0.4	26.5	30.1	-0.3	0.4	37.0	24.3	-0.6	0.6
<b>CESM 0.25d</b>	34.1	26.2	-0.4	0.2	28.1	27.6	-0.4	0.3	26.4	37.4	0.1	-0.7	26.4	37.4	0.1	-0.7	37.6	19.0	-0.5	0.8
<b>CESM 0.125d</b>	34.3	28.5	-0.5	0.4	27.2	30.0	-0.4	0.3	26.3	37.4	0.1	-0.6	26.3	37.4	0.1	-0.6	37.3	21.3	-0.5	0.4
<b>WRF 27km</b>	33.9	34.8	-0.5	0.2	24.9	34.8	-0.3	0.0	26.0	36.7	-0.1	-0.5	26.0	36.7	-0.1	-0.5	36.5	22.6	-0.6	0.5
<b>WRF 9km</b>	32.4	33.1	-0.7	0.6	22.4	38.5	-0.5	0.6	24.9	32.6	0.0	-0.6	24.9	32.6	0.0	-0.6	34.4	24.4	-0.5	0.4

**Notes:** If skew > 0 [skew < 0], the distribution trails off to the right [left]. If kurtosis > 0 [< 0], it is usually more sharply peaked [flatter] than the normal distribution (leptokurtic and platykurtic, respectively).

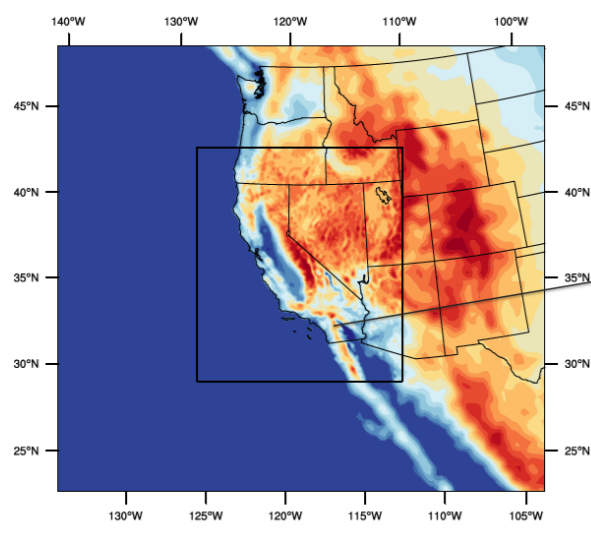
TABLE 4. RMSD, MAD, MRD, Correlation (Corr) for precipitation over California

Annual	CPC				UW				PRISM				DAYMET				
	RMSD	MAD	MRD	Corr	RMSD	MAD	MRD	Corr	RMSD	MAD	MRD	Corr	RMSD	MAD	MRD	Corr	
<b>varres-CESM 0.25d</b>	0.607	0.394	0.413	0.981	0.616	0.292	0.434	0.968	0.727	0.203	0.429	0.952	0.567	0.191	0.375	0.972	
<b>varres-CESM 0.125d</b>	0.469	0.207	0.321	0.980	0.526	0.115	0.339	0.970	0.624	0.045	0.328	0.961	0.504	0.027	0.310	0.973	
<b>WRF 27km</b>	0.419	-0.205	0.269	0.977	0.580	-0.308	0.274	0.971	0.765	-0.396	0.296	0.965	0.647	-0.409	0.312	0.970	
<b>WRF 9km</b>	2.226	1.485	0.950	0.957	2.052	1.393	0.864	0.964	1.889	1.322	0.815	0.970	2.005	1.306	0.773	0.961	
<b>uniform CESM 0.25d</b>	0.555	0.134	0.277	0.969	0.600	0.031	0.302	0.961	0.700	-0.057	0.290	0.953	0.600	-0.069	0.284	0.962	
DJF		CPC				UW				PRISM				DAYMET			
		RMSD	MAD	MRD	Corr	RMSD	MAD	MRD	Corr	RMSD	MAD	MRD	Corr	RMSD	MAD	MRD	Corr
<b>varres-CESM 0.25d</b>	1.486	0.986	0.532	0.972	1.445	0.673	0.531	0.959	1.654	0.577	0.547	0.943	1.346	0.514	0.435	0.964	
<b>varres-CESM 0.125d</b>	1.194	0.638	0.396	0.976	1.234	0.346	0.398	0.965	1.395	0.287	0.400	0.955	1.170	0.212	0.337	0.969	
<b>WRF 27km</b>	0.888	-0.376	0.269	0.975	1.289	-0.688	0.289	0.967	1.552	-0.785	0.298	0.962	1.351	-0.848	0.324	0.966	
<b>WRF 9km</b>	4.264	2.607	0.742	0.950	3.835	2.315	0.616	0.955	3.570	2.256	0.604	0.964	3.804	2.183	0.554	0.955	
<b>uniform CESM 0.25d</b>	1.392	0.377	0.300	0.960	1.431	0.064	0.316	0.951	1.544	-0.033	0.314	0.946	1.406	-0.095	0.288	0.953	

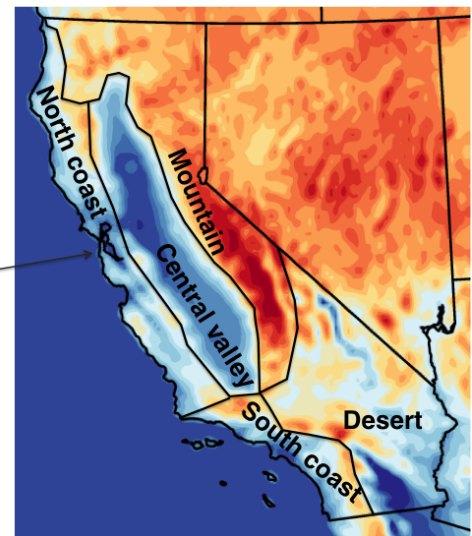
## 726 LIST OF FIGURES

727	<b>Fig. 1.</b> Domains of WRF simulations (left) and five climate divisions in California (right) with topography in meters (m). . . . .	40
728		
729	<b>Fig. 2.</b> Grid meshes for the two varres-CESM simulations. . . . .	41
730		
731	<b>Fig. 3.</b> Topography in meters (m) for (top left to bottom right) varres-CESM $0.25^\circ$ , varres-CESM $0.125^\circ$ , uniform CESM-FV $0.25^\circ$ , WRF 27km, WRF 9km and ERA-Interim ( $\sim 80$ km). . . . .	42
732		
733	<b>Fig. 4.</b> JJA average daily Tmax, Tmin and Tavg from models and reference datasets, and differences between them ( $^\circ\text{C}$ ). . . . .	43
734		
735	<b>Fig. 5.</b> sample standard deviation of JJA average daily Tmax, Tmin and Tavg from models and PRISM ( $^\circ\text{C}$ ). . . . .	44
736		
737	<b>Fig. 6.</b> Seasonal cycle of monthly-average Tavg for each subzone ( $^\circ\text{C}$ ). Bars represent standard deviation ( $\sigma$ ) values. . . . .	45
738		
739	<b>Fig. 7.</b> Seasonal standard deviation ( $s$ ) values of monthly-average Tavg for each subzone ( $^\circ\text{C}$ ). Bars represent standard deviation ( $s$ ) values. . . . .	46
740		
741	<b>Fig. 8.</b> Frequency distribution of summer Tmax ( $^\circ\text{C}$ ). . . . .	47
742		
743	<b>Fig. 9.</b> Annual and DJF precipitation from models and reference datasets (mm/d). . . . .	48
744		
745	<b>Fig. 10.</b> sample standard deviation of Annual and DJF precipitation from models and PRISM (mm/d). . . . .	49
746		
747	<b>Fig. 11.</b> As Figure 6, but for monthly-average total precipitation (mm/d). . . . .	50
748		
749	<b>Fig. 12.</b> As Figure 7, but for monthly-average total precipitation (mm/d). . . . .	51
750		
751	<b>Fig. 13.</b> Frequency distribution of winter Pr constructed from 26 years of daily data (mm/d) (note that the vertical scale is logarithmic). . . . .	52
752		
753	<b>Fig. 14.</b> Taylor diagram of annual climatology for the entire California region, using the PRISM dataset as reference. . . . .	53

WRF 9km : Outer and inner domain

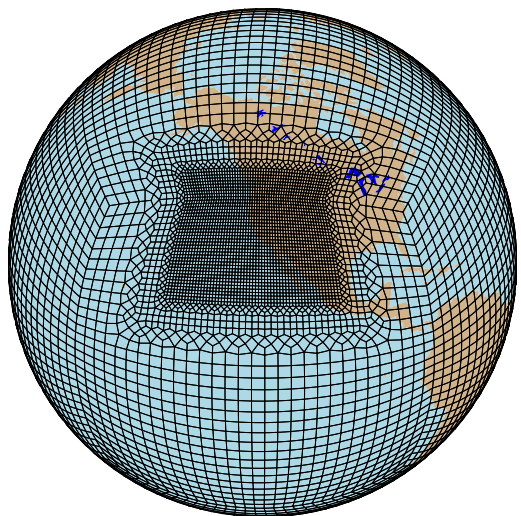


Climate divisions across CA



750 FIG. 1. Domains of WRF simulations (left) and five climate divisions in California (right) with topography in  
751 meters (m).

1 degree -> 0.25 degree



1 degree -> 0.125 degree

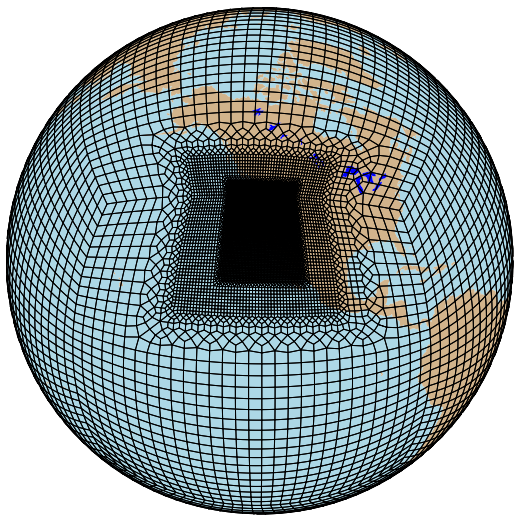
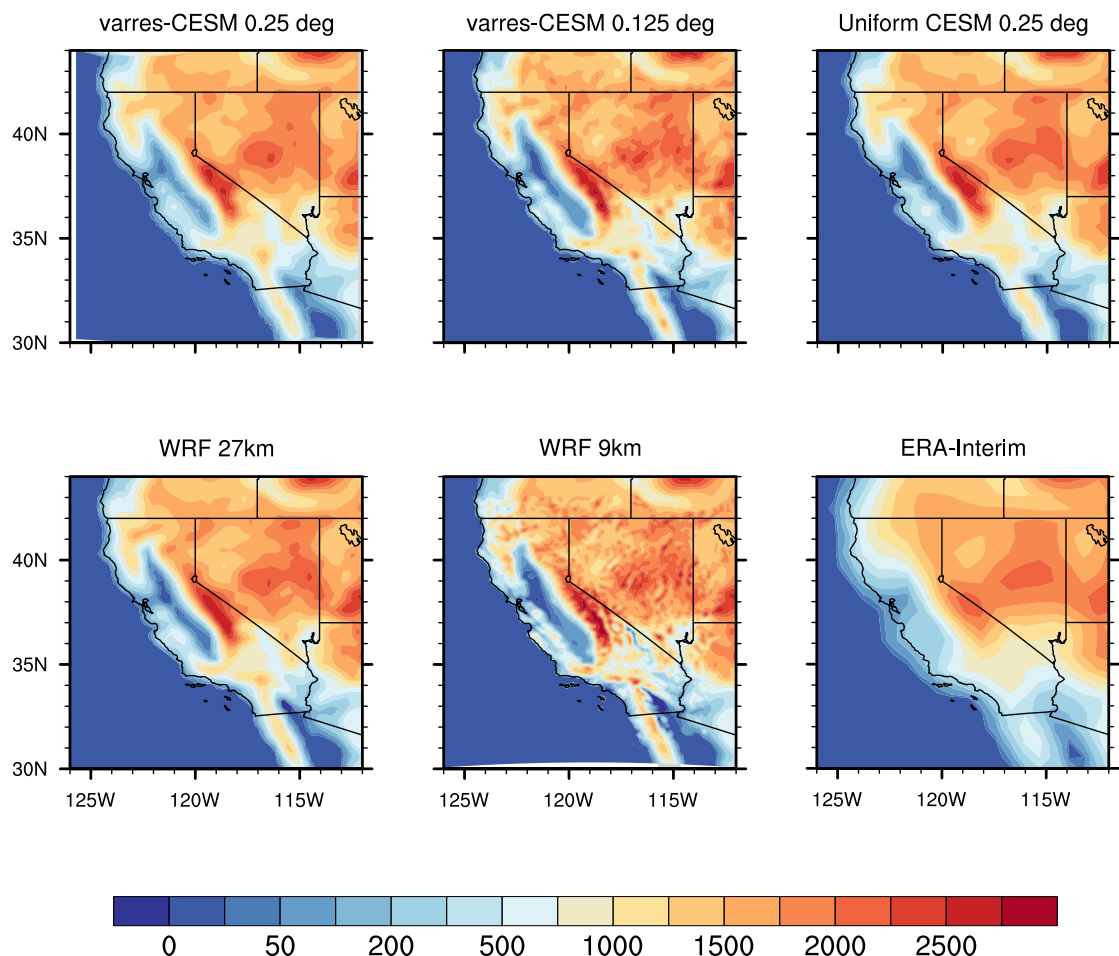
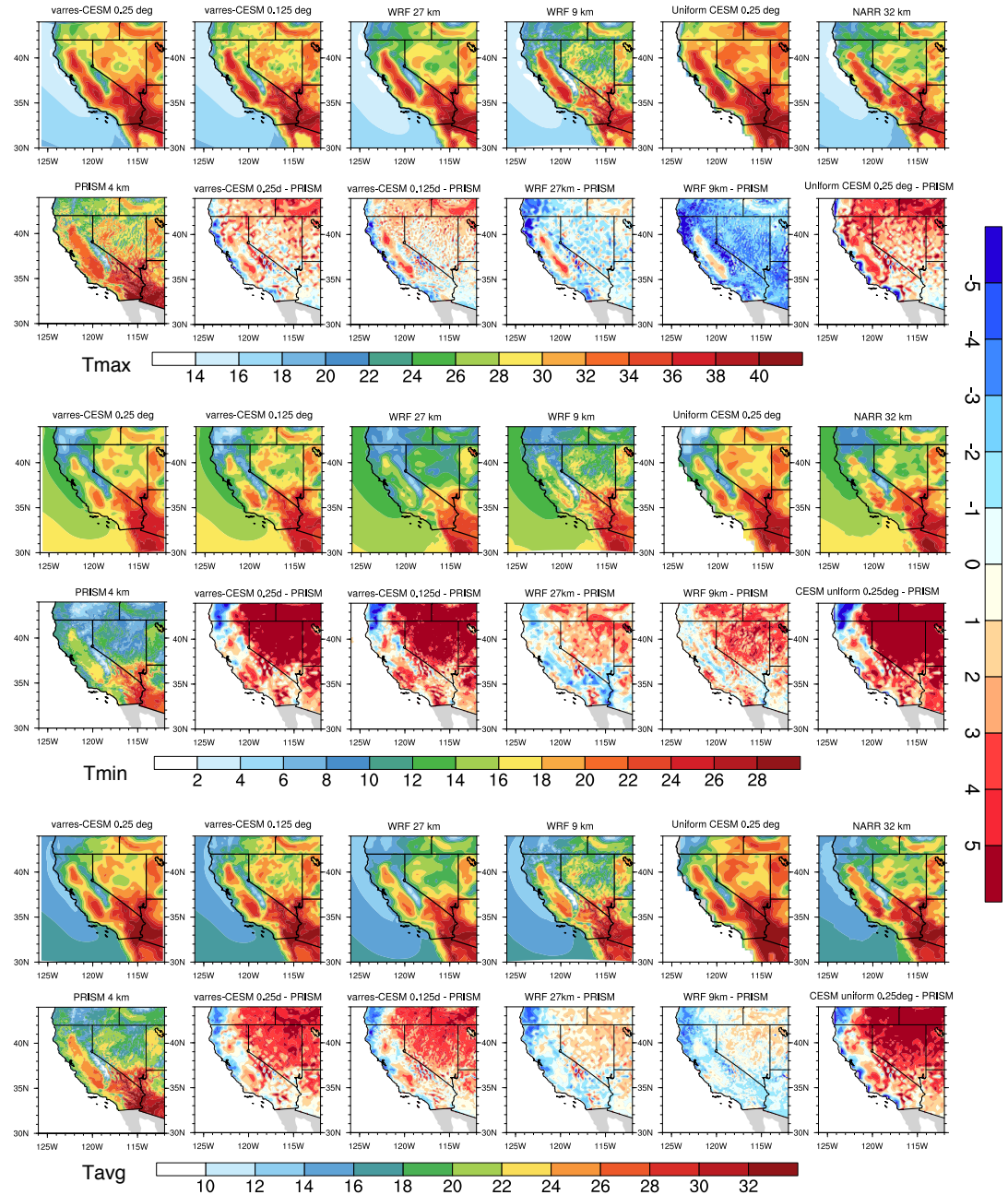


FIG. 2. Grid meshes for the two varres-CESM simulations.



752 FIG. 3. Topography in meters (m) for (top left to bottom right) varres-CESM  $0.25^\circ$ , varres-CESM  $0.125^\circ$ ,  
753 uniform CESM-FV  $0.25^\circ$ , WRF 27km, WRF 9km and ERA-Interim ( $\sim 80$  km).



754 FIG. 4. JJA average daily Tmax, Tmin and Tavg from models and reference datasets, and differences between  
 755 them ( $^{\circ}\text{C}$ ).

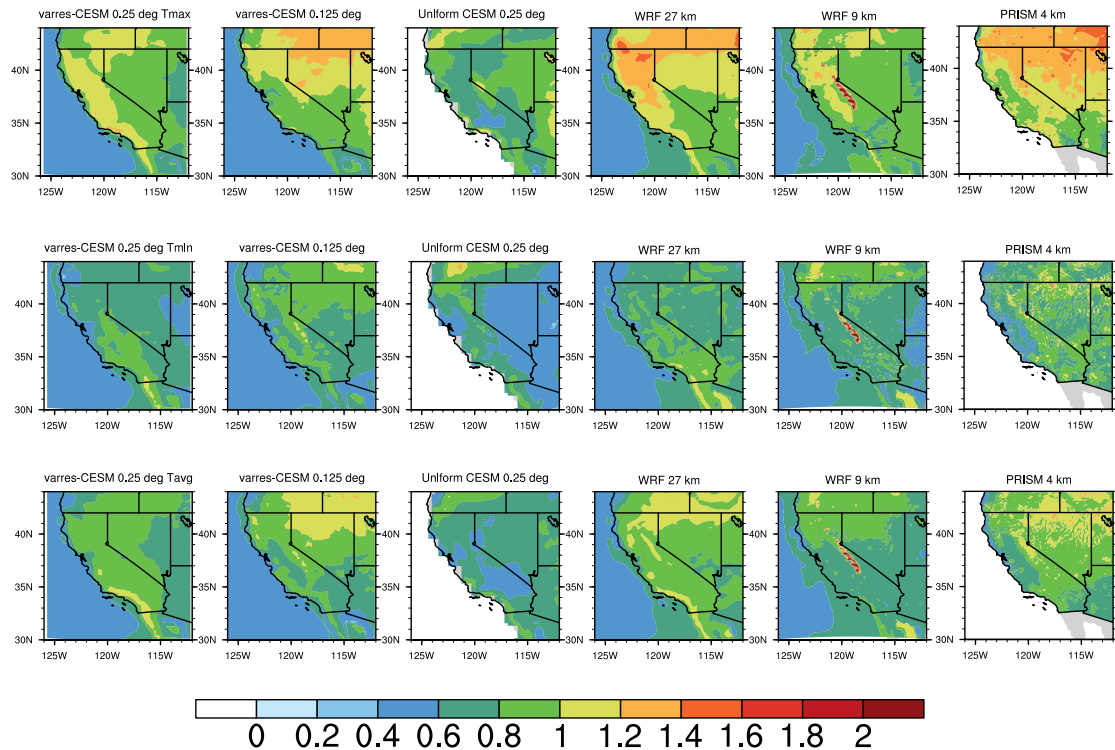
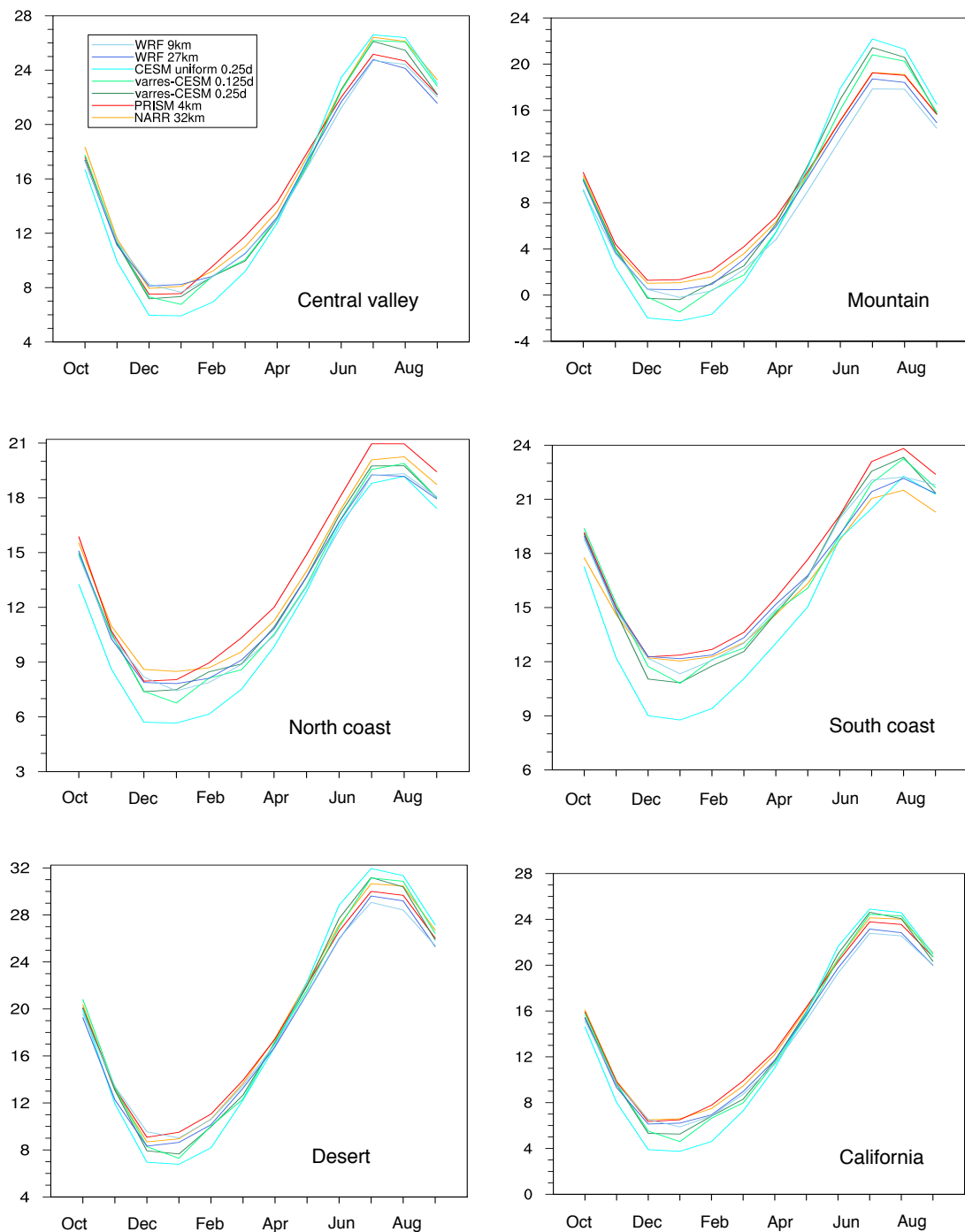
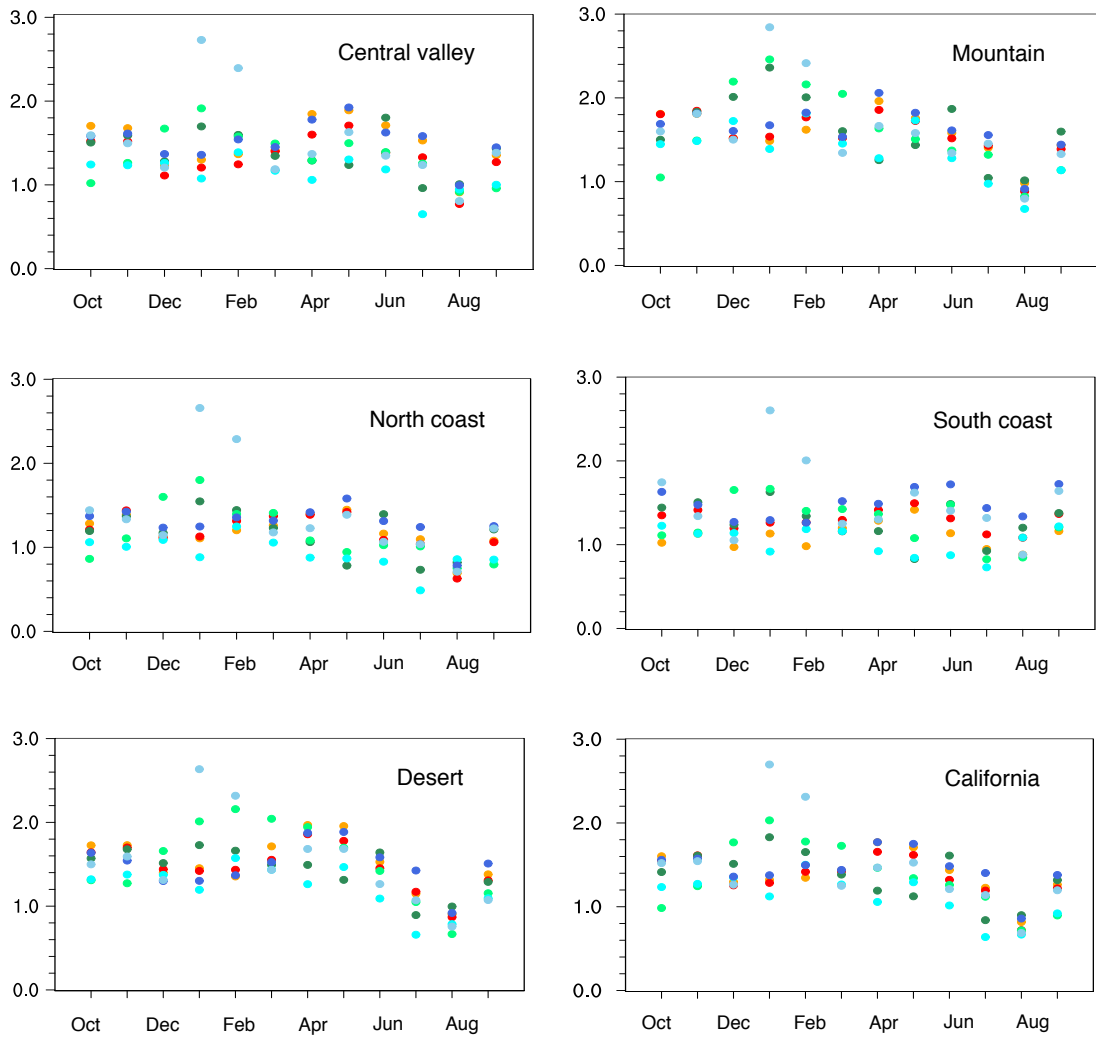


FIG. 5. sample standard deviation of JJA average daily Tmax, Tmin and Tavg from models and PRISM ( $^{\circ}\text{C}$ ).



756 FIG. 6. Seasonal cycle of monthly-average Tavg for each subzone ( $^{\circ}\text{C}$ ). Bars represent standard deviation ( $\sigma$ )  
757 values.



758 FIG. 7. Seasonal standard deviation ( $s$ ) values of monthly-average  $T_{avg}$  for each subzone ( $^{\circ}C$ ). Bars represent  
759 standard deviation ( $s$ ) values.

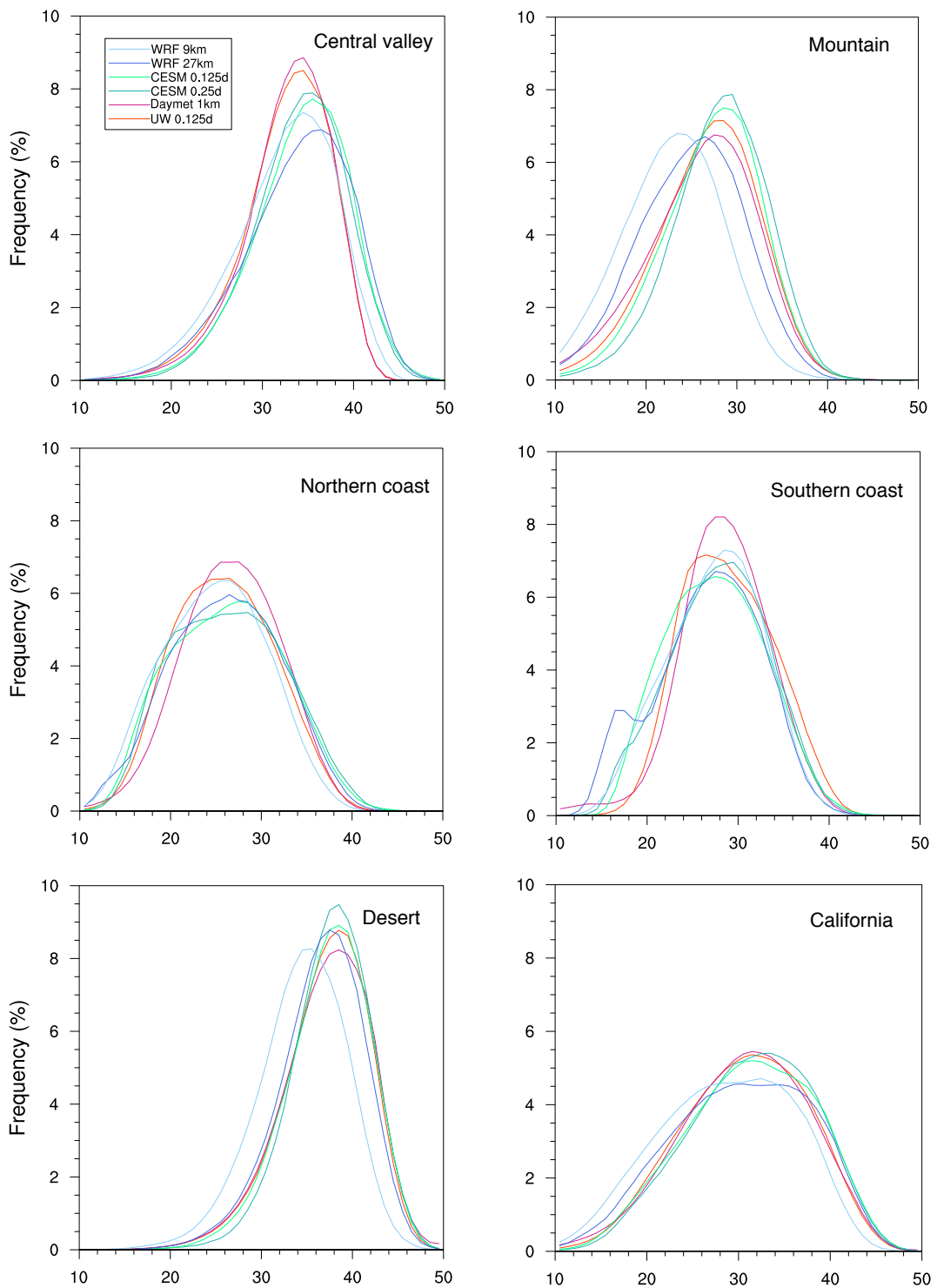


FIG. 8. Frequency distribution of summer Tmax ( $^{\circ}\text{C}$ ).

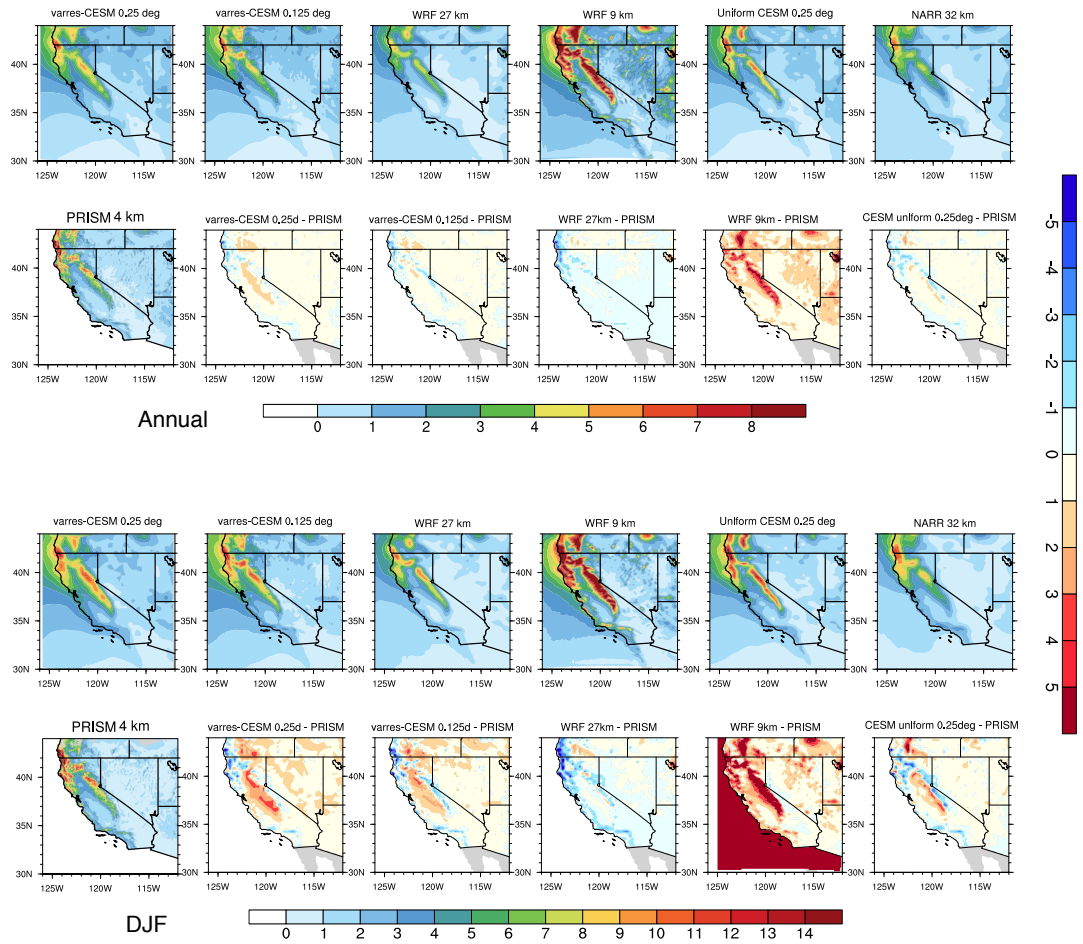


FIG. 9. Annual and DJF precipitation from models and reference datasets (mm/d).

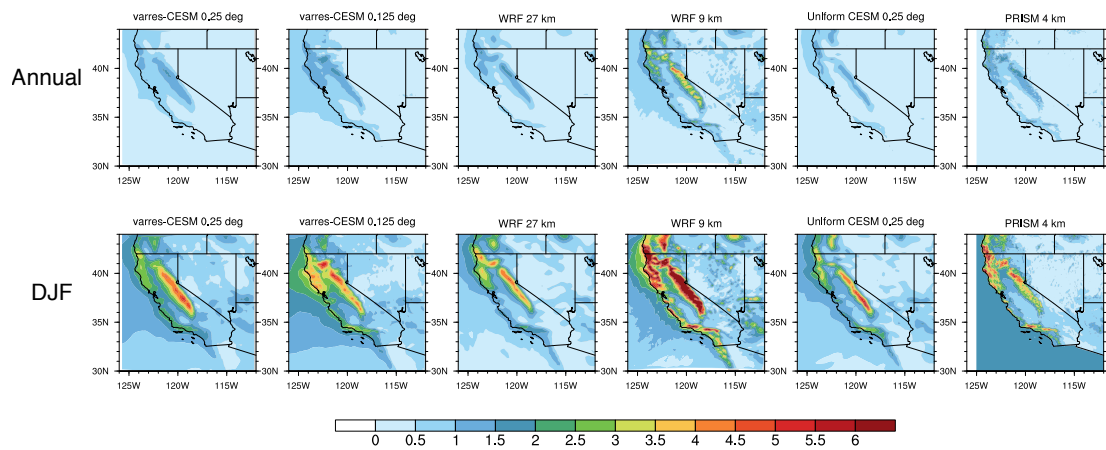


FIG. 10. sample standard deviation of Annual and DJF precipitation from models and PRISM (mm/d).

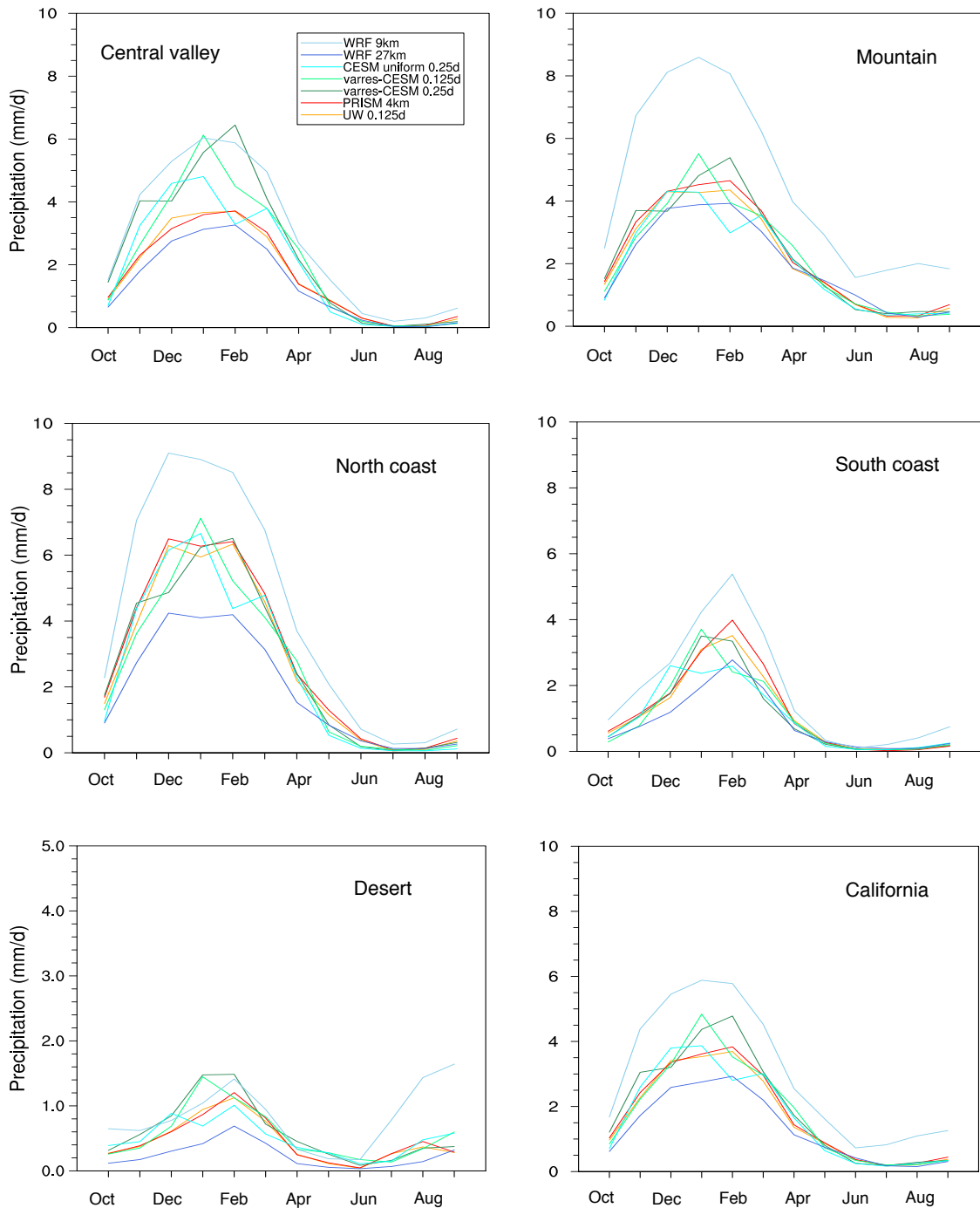


FIG. 11. As Figure 6, but for monthly-average total precipitation (mm/d).

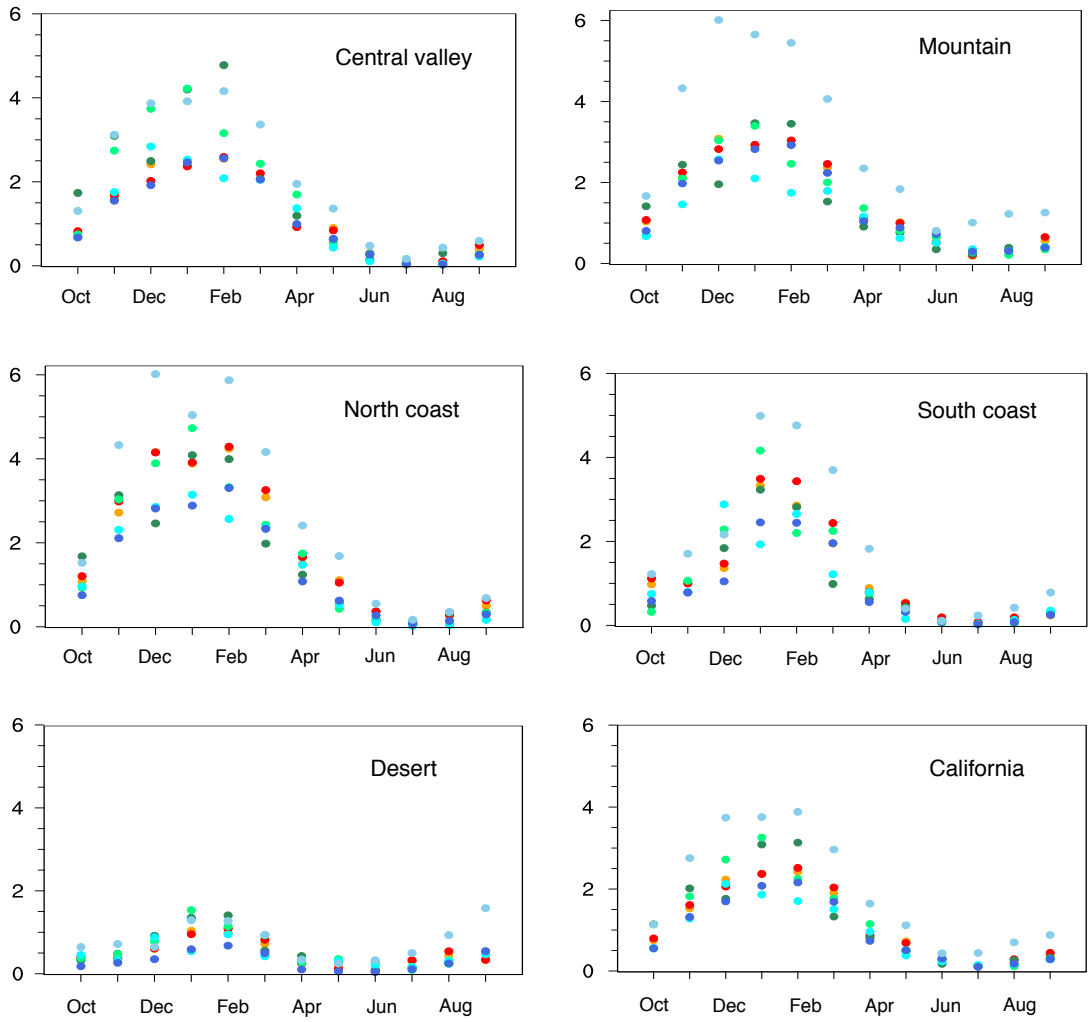
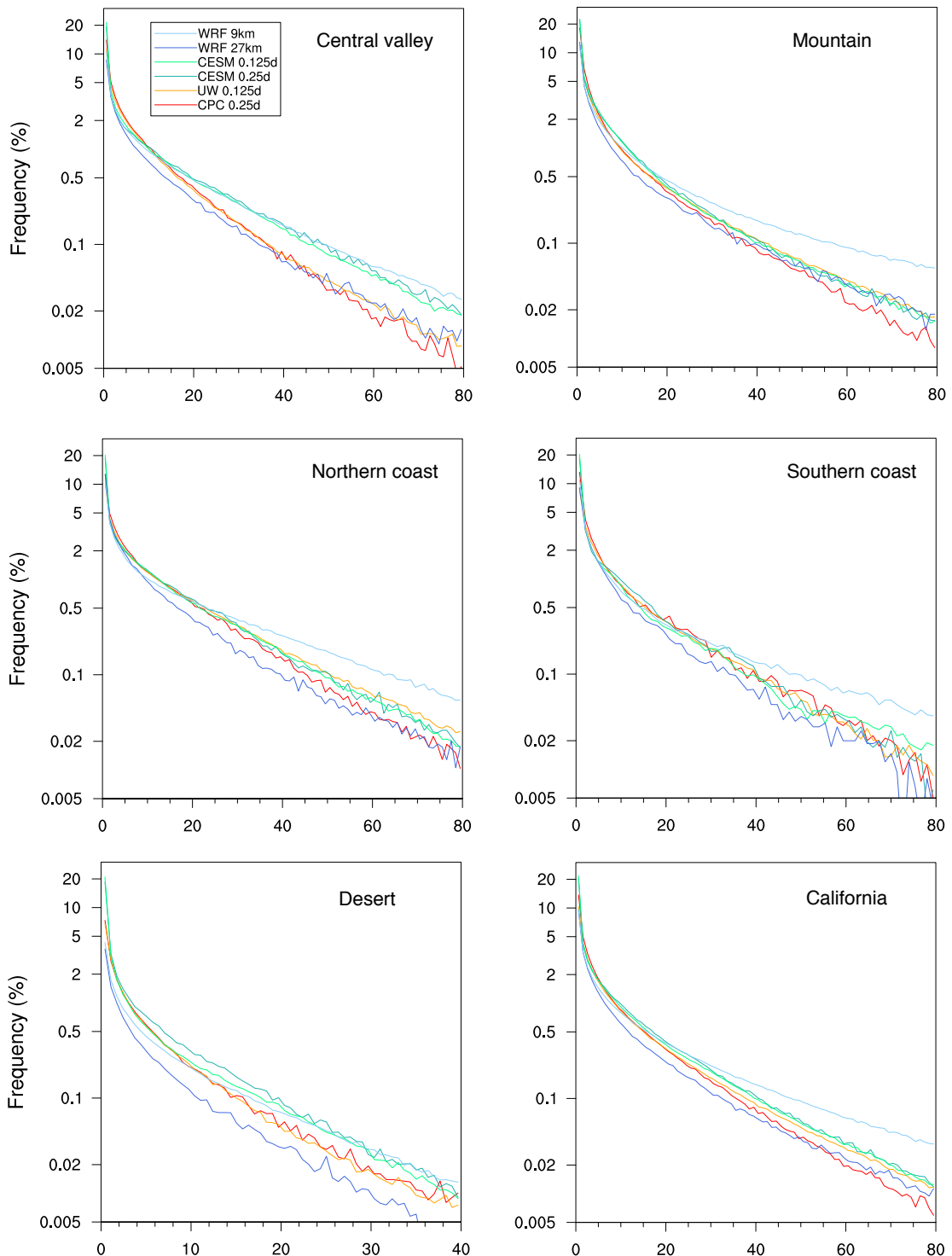
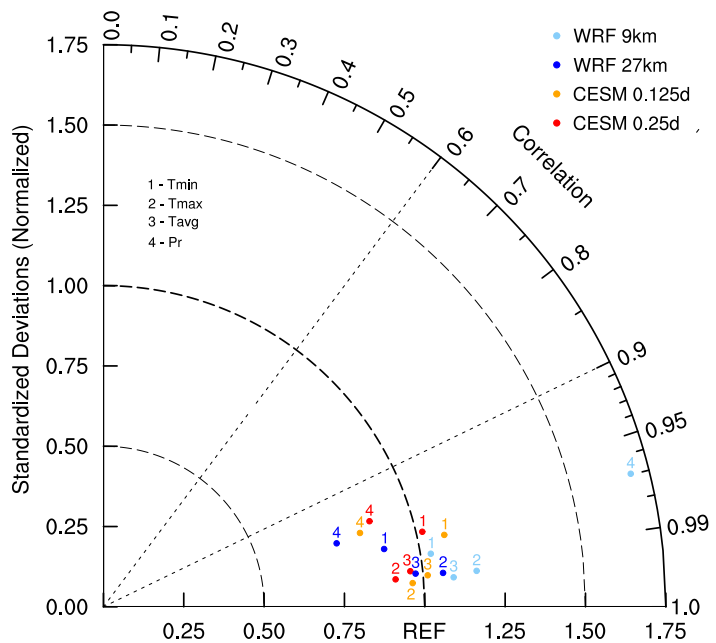


FIG. 12. As Figure 7, but for monthly-average total precipitation (mm/d).



760 FIG. 13. Frequency distribution of winter Pr constructed from 26 years of daily data (mm/d) (note that the  
 761 vertical scale is logarithmic).



762 FIG. 14. Taylor diagram of annual climatology for the entire California region, using the PRISM dataset as  
 763 reference.